Laboratory of Radiochemistry
Department of Chemistry
Faculty of Science
University of Helsinki

Sorption of trivalent actinides onto gibbsite, γ-alumina, and kaolinite

A spectroscopic study of An(III) interactions at the mineral-water interfaces

Nina Maria Huittinen

ACADEMIC DISSERTATION

To be presented, with the permission of the Faculty of Science of the University of Helsinki, for public examination in lecture hall A110, Department of Chemistry, on 22 February 2013, at 12 noon.

Helsinki 2013

Supervised by

Prof. Jukka Lehto
Laboratory of Radiochemistry
Department of Chemistry
University of Helsinki

Prof. Horst Geckeis
Dr. Thomas Rabung
Institute for Nuclear Waste Disposal
Karlsruhe Institute of Technology

Reviewed by

Prof. Stepan N. Kalmykov
Radiochemistry Division
Lomonosov Moscow State University

Dr. Takaumi Kimura
Division of Chemistry for Nuclear Engineering
Nuclear Science and Engineering Directorate
Japan Atomic Energy Agency

Dissertation opponent

Prof. Christian Ekberg
Nuclear Chemistry
Department of Chemical and Biological Engineering
Chalmers University of Technology

ISSN 0358-7746
ISBN 978-952-10-8610-6 (paperback)
ISBN 978-952-10-8611-3 (PDF)
http://ethesis.helsinki.fi

Unigrafia
Helsinki 2013

Sometimes things are hidden under the surface. You just gotta know how to bring 'em out.

-MacGyver

After climbing a great hill, one only finds that there are many more hills to climb.

-Nelson Mandela

Abstract

This Ph.D. thesis concerns investigations on the interactions of trivalent actinides with the mineral phases γ-alumina, gibbsite, and kaolinite. Spectroscopic methods, namely time-resolved laser fluorescence spectroscopy (TRLFS) and nuclear magnetic resonance (NMR) have been employed together with macroscopic sorption investigations to obtain molecular level process understanding of the solid-water interface reactions occurring in the mineral suspensions.

Results obtained in the macroscopic sorption investigations with gadolinium(III) and the spectroscopic (TRLFS) investigations with curium(III) onto the aluminum hydroxide phase gibbsite, α-$Al(OH)_3$ showed that two interaction mechanisms, inner sphere surface complexation and incorporation, are required to explain the metal ion speciation at the gibbsite surface over the investigated pH range 5-11.5. Sorption of Gd^{3+}/Cm^{3+} commences at pH values close to 5 through formation of an inner sphere surface complex. When the pH is raised towards the alkaline pH range another inner sphere complex can be detected from the acquired TRLFS data. The continuous increase of suspension pH, however, also influences the solubility of aluminum with a direct impact on the trivalent metal ion speciation. Upon moving from higher aluminum solubility regions in the acidic pH range towards the solubility minimum at pH 6.3, aluminum hydroxide precipitates from oversaturated solutions and consequently incorporates surface bound curium on the gibbsite surface. When further increasing the pH towards the alkaline pH range, aluminum solubility increases again which results in dissolution of the incorporating precipitate uncovering the curium surface complex. This sorption behavior has not been encountered previously in investigations with other aluminum oxide/hydroxide minerals as sorbent phases for trivalent metal ion attachment. Identification of an incorporated curium species as a consequence of pH variations is a clear proof that mineral surfaces cannot be considered as inert with regard to chemical variations as done in many studies.

In macroscopic (Eu^{3+}) and TRLFS (Cm^{3+}) sorption investigations with kaolinite as sorbent phase, both outer sphere and inner sphere surface complexes could be identified. Outer sphere complexation was pronounced in background electrolyte concentrations of 1 mM $NaClO_4$, while outer sphere attachment was found only for low ($<10^{-7}$ M) europium concentrations on a natural kaolinite batch and not at all in synthetic kaolinite suspensions when 100 mM $NaClO_4$ was used in the experiments. Three inner sphere curium complexes differing only in the degree of hydrolysis were found to dominate the speciation over a large pH range (5.5-11.5). These species were assigned to $>Cm(H_2O)_5^{2+}$, $>Cm(OH)(H_2O)_4^{+}$ and $>Cm(OH)_2(H_2O)_3$ based on fluorescence lifetime data and they correlate very well in terms of emission peak positions and fluorescence lifetimes values to curium species found on other clay mineral surfaces. Above pH 11.5 a further curium complex that could not be assigned to a pure hydrolyzed curium surface complex became prevailing. The TRLFS experiments showed that the dissolution of kaolinite in the alkaline pH-range (>10) resulted in the formation of a ternary complex between surface-sorbed curium and dissolved silicates in solution. Thus, the dissolution of the sorbent phase could again be shown to influence the metal ion speciation verifying the need for

spectroscopic investigations for a correct assignment of the formed complexes at the solid/water interface.

The sorption of diamagnetic yttrium(III) and paramagnetic europium(III) on the various surface hydroxyl groups of γ-alumina (γ-Al_2O_3) and kaolinite was investigated in NMR studies. Upon Eu^{3+}/Y^{3+} attachment onto the mineral surfaces the ^1H NMR signal could be seen to decrease. In difference spectra produced by subtracting the acquired proton spectra of samples with high metal ion concentrations from spectra of clean mineral samples or samples with lower metal ion loadings, a manifold of surface hydroxyl groups influenced by the metal ion attachment to the surface could be identified. These surface groups could be assigned to doubly coordinated Al_2-OH and singly coordinated Al-OH groups on the respective mineral surfaces. In the γ-alumina study the wide distribution of chemically very similar OH protons was attributed to variations in O-H bond lengths and to variations in the Al coordination (Al_{IV}/Al_{VI}). In the kaolinite study removed protons in the metal ion sorption reaction were assigned to singly coordinated Al-OH groups at the kaolinite edge surfaces. In addition, indications of trivalent metal ion attachment to bridging Al-OH-Al groups at the gibbsite-like basal plane of the mineral were obtained.

List of Original Publications

The thesis is based on the following original publications, which are referred to in the text by their Roman numerals (I-V).

I. N. Huittinen, Th. Rabung, J. Lützenkirchen, S. C. Mitchell, B. R. Bickmore, J. Lehto, H. Geckeis: Sorption of Cm(III) and Gd(III) onto gibbsite, α-$Al(OH)_3$: A batch and TRLFS study. *J. Colloid Interface Sci.* **2009**, *332*, 158-164.

II. N. Huittinen, Th. Rabung, P. Andrieux, J. Lehto, H. Geckeis: A comparative batch sorption and time-resolved laser fluorescence spectroscopy study on the sorption of Eu(III) and Cm(III) on synthetic and natural kaolinite. *Radiochim. Acta* **2010**, *98*, 613-620.

III. N. Huittinen, Th. Rabung, A. Schnurr, M. Hakanen, J. Lehto, H. Geckeis: New insight into Cm(III) interaction with kaolinite - influence of mineral dissolution. *Geochim. Cosmochim. Acta* **2012**, *99*, 100-109.

IV. N. Huittinen, P. Sarv, J. Lehto: A proton NMR study on the specific sorption of yttrium(III) and europium(III) on gamma-alumina [γ-Al_2O_3]. *J. Colloid Interface Sci*. **2011**, *361*, 252–258.

V. N. Huittinen, P. Sarv, J. Lehto: A ^{1}H and ^{27}Al NMR investigation of yttrium(III) and europium(III) interaction with kaolinite. *Submitted.*

Author's contribution to the publications I-V

The author has planned and executed the majority of the experimental work for all publications. Some mineral characterizations in publications I, II, III, and V have been done by coauthors or analytics personnel at the Karlsruhe Institute of Technology or the University of Helsinki. Some of the TRLFS investigations in publication III were performed by one of the coauthors. NMR measurements were done together with one of the coauthors in papers IV and V. All manuscripts have been written by the author.

Abbreviations

AFM	atomic force microscopy
An	actinide
DFT	density functional theory
EFG	electric field gradient
Eh	redox potential
FI	fluorescence intensity
FID	free induction decay
FT	Fourier transform
HDPE	high-density polyethylene
ICCD	intensified charge-coupled device
ICP-MS	inductively coupled plasma mass spectrometry
IEP	isoelectric point
KBS-3	kärnbränslesäkerhet-3 (nuclear fuel safety), a high-level nuclear waste disposal concept
K_d	sorption distribution coefficient
Kel-F	polychlorotrifluoroethylene
k_{obs}	fluorescence decay rate
Ln	lanthanide
MAS	magic angle spinning
MilliQ	ultrapure water
NMR	nuclear magnetic resonance
PZC	point of zero charge
RF	radiofrequency
RN	radionuclide
SEM-EDX	scanning electron microscopy-energy dispersive x-ray analysis
SKB	Svensk Kärnbränslehantering AB
SNF	spent nuclear fuel
SSB	spinning sideband
TMS	tetramethylsilane
TRLFS	time-resolved laser fluorescence spectroscopy
TRU	transuranium element
XPS	x-ray photoelectron spectroscopy

Acknowledgements

The research for this work was conducted at the University of Helsinki and the Karlsruhe Institute of Technology from August 2007 to January 2013. I am grateful for the financial support I obtained over the complete duration of this thesis from the Finnish Research Programme on Nuclear Waste Management (KYT2010 and KYT2014). Svenska Tekniska Vetenskapsakademien i Finland is gratefully acknowledged for the travel grant that enabled one of the research periods in Karlsruhe.

This work would not have been possible without the help of numerous people. First of all I owe my gratitude to my supervisors Jukka Lehto, Thomas Rabung and Horst Geckeis who introduced me to the topic of my thesis and have been guiding me throughout the studies. You have believed in my capabilities from day one, and allowed me to grow into an independent scientist. Priit Sarv, I want to thank you for the hours and hours spent at the NMR spectrometer measuring my numerous samples. Thank you for your guidance and your support, it has been a true pleasure to work with you!

Numerous people, both coauthors and analytics personnel at KIT-INE, who have provided me with their ideas and plenty of data over the years, thus, enabling the publication of the five papers included in this thesis, are gratefully acknowledged. My colleagues both here in Helsinki as well as in Karlsruhe are thanked for constructive scientific and non-scientific discussions, for always helping me out and for an excellent atmosphere to work in. Pirkko Hölttä, thank you very much for the years in the same office, for your ideas, for your help when it comes to writing funding applications, or for any other matter I've bugged you about over the years. It has been a great pleasure to share the office with you! Leena Malinen, Miia Pehkonen and Mirkka Sarparanta, thank you for your friendship, the multiple Ph.D. student beer-sessions and for your support.

My best friends Mikko, Nina and Paula, you have no idea how much the weekly "therapy" sessions on the jogging trails have helped me out. I am blessed to have you as my friends! Many thanks go to Pisa and my beautiful goddaughters Ronja and Nea, for always putting a smile on my face. Thank you Annika, Holger, Laura, Luise, Marie, Patric, Tobi, Tom, Thorsten, Silvia, Usche… for making my visits in Karlsruhe a blast! Mamma, Iskä, Anna and Lasse, it is a privilege to have you as my family. Even though you might not have contributed to the contents of this thesis, the years of my scientific nerdiness have been greatly balanced by time spent together.

Finally, I want to thank Moe for everything: for reading through and commenting on my manuscripts, for listening to my talks and complaints, for the laughs together, for simply being there. You're making life that much more fun!

Helsinki, January 2013 Nina Huittinen

Table of Contents

1 Introduction

Altogether 435 nuclear power reactor units were operating world-wide in July 2012. The energy produced by these power plants amounts to nearly 20 % of the total energy production in the world, and to approximately a third of the energy production in Europe. In the majority of reactors nuclear energy is obtained from the fission of ^{235}U through bombardment of the uranium nucleus with thermal neutrons. As a neutron is absorbed by the fissile ^{235}U isotope it splits the nucleus into two lighter nuclei of similar masses (fission products) and nuclear energy is released. The neutron absorption by uranium isotopes present in the fuel may also result in the formation of heavier, so called transuranium elements (TRUs). When the fuel is depleted on the ^{235}U isotope and the fission chain-reaction has ceased, the uranium matrix, fission products and transuranium elements accumulated in the fuel rods are discarded. This spent nuclear fuel is currently being stored at the nuclear power plants or sent to nuclear fuel reprocessing sites for recycling.

Finland has chosen to dispose of the nuclear waste without reprocessing in a deep underground nuclear waste repository in the bedrock in Olkiluoto. A number or natural and engineered barriers have been designed for the repository to minimize the risk of radionuclide migration to the biosphere once the repository has been closed. However, to ensure isolation of the radiotoxic elements for sufficiently long times to render the waste harmless, a thorough nuclear safety assessment has to be performed to account for possible release scenarios. This opens challenging research topics for scientists world-wide that not only comprise an immense amount of research covering a wide area of science but also involve work with radioactive substances that require specially designed laboratories and equipment.

The results presented in this thesis may be used for performance assessment concerning the interaction of trivalent actinides with naturally occurring mineral phases. The primary goal of this study has been to obtain new molecular scale data for mechanistic modeling of radionuclide transport in geological environments and to introduce new spectroscopic methods for the study of actinide interactions with mineral surfaces. The majority of the research has been conducted with the trivalent actinide curium(III) or its lanthanide analogues gadolinium(III) and europium(III). The transition metal yttrium(III) has further been used in nuclear magnetic resonance (NMR) spectroscopy investigations due to its diamagnetic properties. The mineral phases γ-alumina (γ-Al_2O_3), gibbsite (α-$Al(OH)_3$) and kaolinite ($Al_2Si_2O_5(OH)_4$) chosen for the study, can be considered as model mineral phases for more complex rock and backfill materials found in a nuclear waste repository. Pure aluminum oxides/hydroxides are scarce rock or backfill components and, thus, of minor direct importance in the context of nuclear waste disposal, but they contain reactive aluminol groups that are present at the surfaces of abundant aluminosilicates in natural

systems. Furthermore, aluminum oxides/hydroxides are isomorphous model phases for trivalent iron oxides and hydroxides. Iron-bearing mineral phases with strong sorption capacities occur both as natural minerals in various rock types and as corrosion products of iron-containing storage containers. In contrast to iron oxides/hydroxides the aluminum minerals show no absorption in the visible light region, thus, allowing for time-resolved laser fluorescence spectroscopy (TRLFS) experiments. Kaolinite on the other hand is one of the main secondary clay minerals found in the water-conducting fissures of the bedrock in Olkiluoto. Moreover, the mineral is an excellent model phase for spectroscopic investigations, due to its simple structure and limited interlayer reactivity.

Trivalent actinide retention and speciation in these three selected mineral environments have been studied by a combination of techniques. Macroscopic sorption investigations together with TRLFS have provided a very good insight into the sorption characteristics, such as sorption mechanisms, complex structures, and the number of An^{3+}/Ln^{3+} species on the different mineral phases. In addition, NMR investigations have provided information on the various surface hydroxyl groups involved in the complexation reactions of the trivalent metals on the mineral phases γ-alumina and kaolinite. NMR has not been applied for these types of experiments before and these unique investigations generate new experimental data to explain reactions of trivalent actinides at solid/water interfaces.

2 Final disposal of spent nuclear fuel

The disposal of radioactive waste in deep geological repositories was brought up already in the 1950s [1]. Today the concept has evolved with the growing need for safely containing the increasing amounts of radioactive waste originating from nuclear power plants and reprocessing facilities. With a nuclear waste management plan, the world's first permanent nuclear waste repository on its way, and a fixed schedule for waste burial and closure of the repository, Finland is a pioneer in the field of nuclear waste disposal. The bedrock in the Scandinavian shield in Finland, at a depth of ca. 400 m, will serve as host rock for the repository [2]. The waste will be secured through a multi-barrier system which is expected to ensure that the spent nuclear fuel (SNF) and the radiotoxic elements therein cannot be released to the biosphere or become available for humans. This multi-barrier final disposal solution is based on the KBS-3 model developed by Svensk Kärnbränslehantering AB (SKB) [3]. Here the SNF, which mainly consists of UO_2 with a very low solubility under reducing repository conditions, will be encapsulated in canisters consisting of an inner cast iron insert contributing to the mechanical durability of the canister and an outer corrosion-resistant copper layer (technical barrier). The canisters will be placed in deposition holes which will be bored in the floors of several deposition tunnels and void space will be filled with bentonite clay (geotechnical barrier) that swells upon contact with water. Thus, the bentonite clay will prevent water from moving around the canister and protect the canister from possible rock movement. The tunnels will be backfilled with a mixture of bentonite and crushed rock to ensure that the canisters and their bentonite protection will remain in place in the deposition holes and that water inflow is precluded [4]. Finally, should radionuclides from the SNF escape the abovementioned designed barriers through migration with ground water, radionuclide interactions with rock and mineral surfaces in the surrounding bedrock will serve as important retardation mechanisms for the further migration of these radiotoxic elements in the geosphere (geological barrier). To ensure total isolation of radioelements from the biosphere the disposal of SNF must be accompanied by thorough safety assessments comprising both the natural and engineered barriers as well as natural phenomena such as earthquakes and ice age cycles. Such safety assessments become very challenging as they must embrace time-scales of hundreds of thousands of years due to the radiotoxicity of the most long-lived elements in the SNF. In most nuclear waste forms, such long-lived radiotoxic elements are the transuranium elements (TRU) Np, Pu, Am, and Cm, Figure 1 [5-7]. Understanding the geochemistry of these elements is, therefore, crucial for the safety assessment of any repository design.

In the present thesis the TRUs in the valence state +III, mainly Am^{3+} and Cm^{3+}, have been focused on. Due to the reducing conditions in an underground storage site the trivalent state can be expected to be of particular importance. It is the most stable oxidation state for Am and Cm, and it is also expected that significant fractions of plutonium will be

present in the trivalent state. The aim of the work has been to understand the reaction mechanisms controlling the attachment of these elements onto chosen mineral phases and their speciation on the mineral surface over a broad pH-range. The relevant aspects of actinide geochemistry and the speciation methods are, thus, discussed in the following chapters.

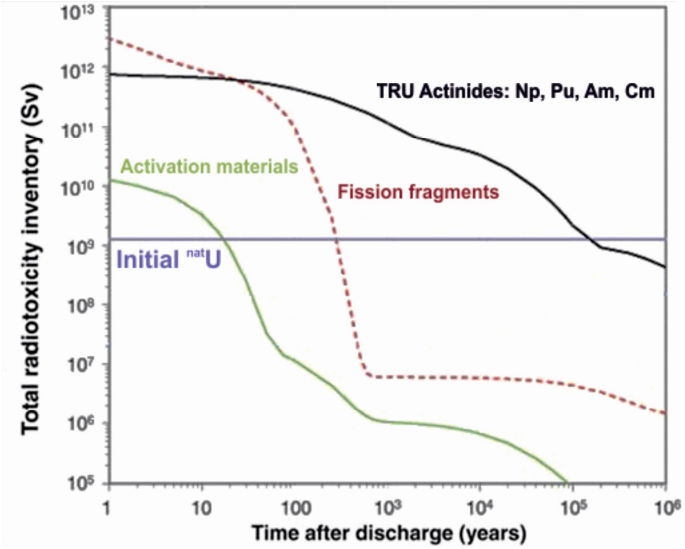

Figure 1: The radiotoxicity inventory of SNF is governed by the transuranium elements Np, Pu, Am and Cm once the short-lived fission products have decayed. Figure adapted from [7].

3 Actinide geochemistry

The main transport path for radionuclides (RNs) from the final disposal site towards the biosphere is the migration with groundwater. The speciation of radionuclides and, thus, their solubility and migration properties is directly correlated to groundwater parameters such as the temperature, pH, redox potential (Eh), and the chemical composition in terms of dissolved inorganic and organic species. Consequently, the basis for the aqueous geochemistry of radioelements must be a comprehensive understanding of their aqueous chemistry. The formation of complexes with inorganic and organic ligands, radionuclide interaction with mobile solid phases (colloids) and the formation of intrinsic colloids are all processes that may affect radionuclide migration in the geosphere. Immobile solid phases such as the host-rock surrounding the SNF repository will, on the other hand, immobilize the RNs or impede their migration in the groundwater by providing sorption sites for RN attachment. A sound understanding of these solid/water interface reactions is of fundamental importance for the safety assessment of nuclear waste repositories. In the following sections hydration, hydrolysis, and the complexation of metal ions with inorganic ligands, which are the most relevant aqueous processes of trivalent actinides in the framework of this thesis, will be discussed as well as different sorption mechanisms on solid surfaces and their implication for trivalent actinide immobilization in the geosphere.

3.1 Aquatic chemistry

3.1.1 Hydration of metal cations

Knowledge of the properties of hydrated ions is important for understanding the chemistry of these ions in aqueous solutions. Hydration is also one of the key phenomena dictating the spectroscopic properties of the curium(III) ion as discussed in Section 4.1. Hydration involves bonding of water molecules to a charged atom or molecule. In case of metal cations, their positive charges attract and become attracted by oxygen atoms of dipolar water molecules in solution. The greater the charge of the metal ion, the stronger is the attraction and consequently the bond formation between the intact water entities and the metal cation in solution. These hydrated metal cations are referred to as aquo complexes or aquo ions with the generic formula $[M(OH_2)_N]^{z+}$ [8]. Here, N, referred to as the hydration number, is the number of H_2O entities in the first coordination sphere of the metal ion, i.e. the number of water molecules directly associated with the metal in solution. This number is to a great degree dependent on the size of the cation, but no explicit rule that would be applicable to all metals in the periodic system exists and, thus, N has to be determined individually for each element.

The hydration number of Cm^{3+} has been investigated using a number of experimental methods [9]. In time-resolved laser fluorescence spectroscopy (TRLFS) studies measurements of the Cm^{3+} fluorescence decay constant as a function of residual hydration in curium-doped crystals of lanthanide complexes yields a value of 9.2 ± 0.5 H_2O entities in the first coordination sphere of Cm^{3+} in water [10]. Lindqvist-Reis et al. [11] showed that the Cm^{3+}(aq) spectrum can be described by an equilibrium between octa- and nonahydrated species with molar ratios of 1:9 at 20°C. Single-crystal X-ray diffraction of $Cm(H_2O)_9(CF_3SO_3)_3$ has further been employed to understand the hydration of Cm^{3+} in solution [12-13]. In these studies curium was found to coordinate to nine water molecules with a tricapped-trigonal-prismatic geometry. Finally, a primary hydration number of 9 for the curium aquo ion has been confirmed in density functional theory (DFT) calculations, Figure 2 [14].

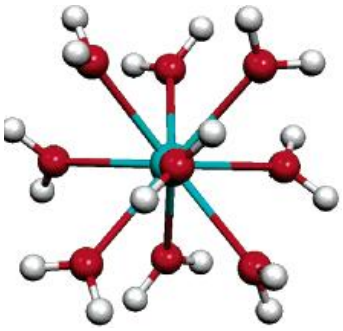

Figure 2: In solution the curium(III) cation is surrounded by nine water molecules in the first coordination sphere [14]. This hydrated ion is referred to as the curium aquo ion.

The f-elements form small, highly charged cations. The large charge density leads to a very strong hydration, as described for Cm^{3+}. This strong hydration competes with complexation reactions by ligands as the process of complexation involves the displacement of one or more water-molecules by the ligand [15]. Such reactions, involving hydrolysis and complexation with other inorganic ligands will be discussed in the following sections.

3.1.2 Hydrolysis

The strong attraction between positive f-element cations and the negatively charged oxygen atom in the water molecule polarizes the O-H bond in water, making it more acidic and consequently more prone to dissociation. This process is referred to as hydrolysis. The ability of hydrated metal ions to hydrolyze depends on their effective charge and size. A small metal cation with high effective charge (e.g. Al^{3+}, Si^{4+}) is more strongly hydrolyzed than a big metal cation with low effective charge (e.g. Rb^{+}, Sr^{2+}) [16]. For the actinides that appear with stable oxidation states between +III and +VI in aqueous solution the tetravalent oxidation state has the strongest tendency toward hydrolysis, while

the pentavalent one has the weakest. This is due to the instability of the highly charged pentavalent and hexavalent actinides in aqueous solution that form linear trans-dioxo cations AnO_2^+ and AnO_2^{2+}, respectively, the so-called actinyl ions. The covalent bonding between the metal and the two oxygen atoms reduces the effective charge of the actinide ion to 2.3 ± 0.1 for An(V) and 3.2 ± 0.1 for An(VI) [15, 17]. Thus, the charge density and in conclusion the tendency toward hydrolysis of actinide ions decreases in the series An^{4+} > AnO_2^{2+} >An^{3+} > AnO_2^+ [9, 18]. Hydrolysis occurs due to polarization of the attached water molecules by the positively charged hydrated actinide species $An(H_2O)_x^{z+}$ or $AnO_2(H_2O)_x^+$ and $AnO_2(H_2O)_x^{2+}$ that weakens the O-H bonds sufficiently to release protons to the surrounding solution [9]. As the reaction involves proton dissociation, hydrolysis increases with increasing pH. The hydrolysis reactions for the actinide elements occur in very acidic (tetravalent state) to mildly alkaline (pentavalent) solutions and they can be expressed by the general Equation 1:

$$nAn^{z+} + xH_2O \leftrightarrow An_n(OH)_x^{nz-x} + xH^+ \quad (1)$$

where An stands for An^{3+} and An^{4+} in the case of tri- and tetravalent actinides or AnO_2^+ and AnO_2^{2+} in the case of penta- and hexavalent actinides [9]. In Figure 3, the pH dependence of the hydrolysis reaction is illustrated for the trivalent curium ion. The trivalent actinide forms neutral or positively charged metal-hydroxo complexes of the generic formula $Cm(OH)_x^{3-x}$, where x = 1-3 [19]. The figure is only applicable for pure water where OH^- is the sole anionic ligand present and for curium concentrations where the solubility limit of $Cm(OH)_3$ (s) is not exceeded.

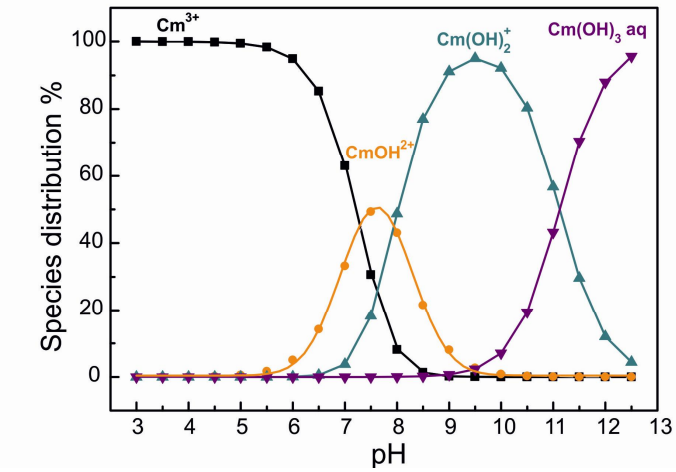

Figure 3: The distribution of curium(III) hydrolysis species in solution as a function of solution pH. The solution speciation was calculated using the PhreeqC modeling code [20] and the ANDRA ThermoChimie v.7b database [21].

Below pH 6 (and under the constraint discussed above) the hydrated curium aquo ion is the sole species in solution. When the pH is increased to 6 and above the formation of the

hydrolysis complex $CmOH^{2+}$ occurs, followed by the second hydrolysis complex $Cm(OH)_2^{+}$. Above pH 8.5 no unhydrolyzed curium exists in solution. The neutral hydroxo complex $Cm(OH)_3$ (aq) becomes prevailing above pH 11.

3.1.3 Complexation with other inorganic ligands

Besides the hydroxyl ligand, other inorganic anionic species and organic compounds present in the ground water may form complexes with dissolved cationic RNs. Inorganic ligands comprise e.g. carbonates (CO_3^{2-}), sulfates (SO_4^{2-}), phosphates (PO_4^{3-}), nitrates (NO_3^{-}), halides (Cl^{-}, Br^{-}, F^{-}, I^{-}) and silicates (SiO_4^{4-}) [22-24], while important organic components in the water with strong complexing properties are e.g. biodegradation products such as humic and fulvic acids [25]. These organic compounds, even though very important for the fate or RN in the geosphere, have not been a subject of study in this work and will, thus, not be discussed further.

The presence of inorganic ligands in the deep underground is mainly determined by the composition and dissolution of surrounding mineral phases and dissolved gases. In the deep underground of the final disposal site for SNF in Olkiluoto, Finland, calcite, iron sulfides (mainly pyrite) and the clay minerals chlorite, illite and kaolinite have been found to predominate as secondary fracture minerals [26-28]. The clay mineral coatings are among the most frequent infills of the water-conducting fractures in the bedrock [29]. The dissolution of these minerals increases the amount of anionic ligands such as carbonates and silicates in the surrounding ground water in which chloride (Cl^{-}) has been found to be the most abundant anion [29]. The carbonate ligand is a very strong inorganic complexing agent of dissolved actinides in all oxidation states whereas the actinides form very weak complexes with chloride [19, 30]. Reported data on the complexation of actinides with dissolved silicates is scarce. Jensen and Choppin [31], showed that silicic acid can be an important ligand in mildly acidic or neutral waters for the complexation of europium(III), taken as an analogue for trivalent actinide elements. They could identify the Eu-silicate complexes $EuOSi(OH)_3^{2+}$ and $Eu[OSi(OH)_3]_2^{+}$ in solutions containing orthosilicic acid, $Si(OH)_4$, and stability constants for both the 1:1 and 1:2 complexes could be derived by TRLFS. For trivalent actinides such as Am^{3+} and Cm^{3+} only the 1:1 silicate ($AmOSi(OH)_3^{2+}$ and $CmOSi(OH)_3^{2+}$) complex has been identified in solution and a formation constant derived for the complex [32-35]. Nevertheless, other Ln^{3+}/An^{3+}-silicates have been encountered in e.g. Panak et al. [33] and Wang et al. [34]. These silicate species could not be assigned to the 1:2 complex but rather to Cm^{3+} attachment to colloidal silicates ($pH \leq 9$) [33] or to Eu^{3+}/ Cm^{3+} complexation with polysilicates in basic solutions (pH 12) [34]. Within the framework of this thesis, Cm^{3+} complexation reactions with dissolved silicates in alkaline kaolinite environments were found to dominate the metal ion speciation through formation of ternary curium-silicate complexes on the clay mineral surface (Article III). Surface complexation reactions will be discussed in detail in the following section.

3.2 Reactions at the mineral/water interface

Sorption of radionuclides on mineral surfaces is regarded as one of the dominant retardation processes in the near and far-fields of nuclear waste repositories [36, 37]. The term sorption is used to describe the uptake of an ion or compound on solid surfaces, resulting in the transfer of this species from the liquid to the solid phase. Adsorption, incorporation and surface precipitation can be regarded as the most important sorption processes, of which only the two former ones are of relevance to the present work. In adsorption the metal ion is attached to the mineral surface either physically via electrostatic interactions (dipole-dipole, ion-dipole, van der Waals interactions) or chemically via a chemical bond between the ion and the mineral surface [38, 39]. Physical adsorption results in the formation of an outer sphere complex where the metal ion retains the hydration sphere upon attachment to the surface. In inner sphere complexation the metal ion loses parts of its hydration shell to allow for a chemical bond to form between the sorbate and the sorbent [40]. Incorporation on the other hand involves uptake of the ion within the mineral structure. This incorporation mechanism can either involve the direct substitution of the metal ion with one of the mineral's structural components or a non-specific attachment within the mineral structure where no substitution occurs [41]. Adsorption in terms of outer sphere and inner sphere complex formation and incorporation are illustrated in Figure 4.

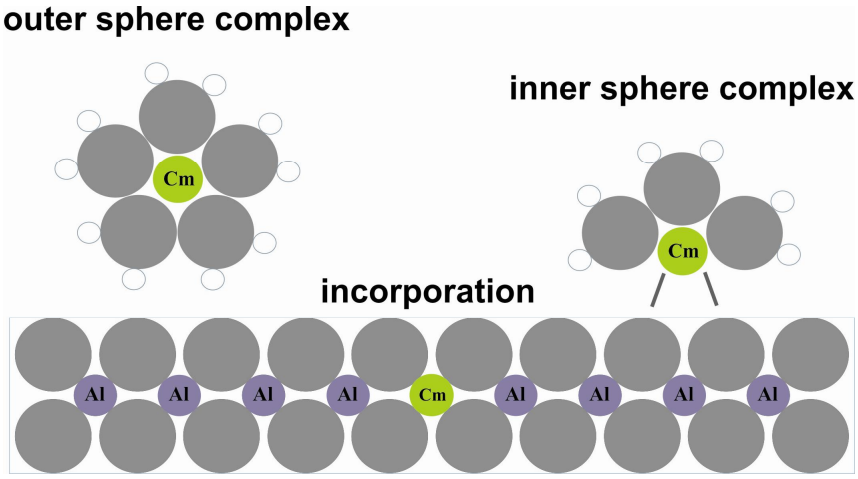

Figure 4: Adsorption of metal ions on a mineral surface can occur through outer sphere or inner sphere complex formation. In incorporation the metal ion uptake occurs within the mineral structure.

It is very important to distinguish among physical sorption, chemical sorption and incorporation reactions as they involve solid/solute interactions of very different strengths and will affect an ion's mobility in different ways. The electrostatic attachment of a RN on a solid surface is very sensitive to variations in the ionic strength of the surrounding solution. An outer sphere metal cation competes with other cations in solution for the negatively charged surface sites [39, 42]. Thus, an increase in ionic strength only, may cause the outer sphere complex to desorb from the surface. Inner sphere complexes are

bound much stronger owing to the chemical bond between the attached metal cation and the solid surface. A change in ionic strength only is usually not sufficient for desorption to occur even though a dramatic increase of potential complexing ligands, such as Cl^-, CO_3^{2-}, SO_4^{2-}, and H_4SiO_4 may increase the amount of RN-ligand complexes in the solution. These complexes, however, can also be formed on the surface (ternary surface complexes) and do not increase the mobility of the RN in the geosphere [43-45]. Under these circumstances changes in the solution pH conditions are required for the detachment of the inner sphere sorbed RN. Finally, incorporation reactions may be very stable retention processes as they involve sorption of the RN within the mineral structure. Dissolution of the material itself and the subsequent release of the RN are usually required for mobilization of the RN in the geosphere [41].

3.2.1 The mineral surface

A common way of describing mineral surface chemistry is by introducing generic hydroxylated surface groups, S-OH [46]. The S-OH groups have amphoteric character and can act as both acids and bases depending on the pH of the solution:

$$S-OH_2^+ \xleftrightarrow{H^+} S-OH \xleftrightarrow{H^+} S-O^- \qquad (2)$$

The surface charge of the mineral is in many cases controlled by this amphoteric reaction of the surface hydroxyls. At low pH, protonated hydroxyl groups dominate and the surface charge is positive, while an increase of solution pH yields increasing amounts of deprotonated sites, leading to an inversion of surface charge. At a certain pH value, the net surface charge will be zero. This point is referred to as the point of zero charge (PZC) or, in very dilute solutions where the adsorption of other ions beside H^+/OH^- can be neglected, the isoelectric point, IEP [40, 47]. The configurations of the different types of surface groups depend on the crystal structure of the mineral but also on the crystal face being studied. The surface hydroxyls can be coordinated to one, two, or three underlying metal atoms and one underlying metal atom may coordinate to multiple surface hydroxyls. The different hydroxyls groups may have very different chemical properties which in turn affects RN sorption onto the different surface sites. In addition, chemically very similar surface hydroxyls can have slight differences in cation-anion bond lengths, e.g. as a consequence of surface relaxations, that may lead to changes in reactivity [48].

Surface groups on γ-alumina, gibbsite, and kaolinite

The aluminum oxide and hydroxide minerals γ-alumina and gibbsite, respectively, and the clay mineral kaolinite used as sorbent phases in the present work all form flat, hexagonal crystals with large basal planes, Figure 5. Despite the similar particle shapes these aluminum bearing mineral phases have different surface hydroxyl configurations. The gibbsite bulk structure consists of stacked sheets of linked octahedrons where every central Al^{3+} cation is coordinated to six oxygen atoms. At the large basal plane of the

mineral, surface hydroxyls coordinated to two aluminum atoms (Al_2-OH) are the sole species present. The platelet edges on the other hand consist of equal amounts of doubly coordinated and singly coordinated (Al-OH) hydroxyls [49].

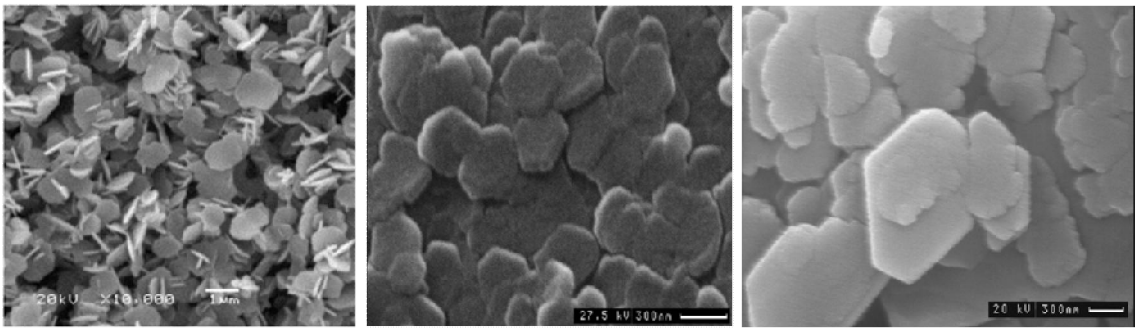

Figure 5: Hexagonally shaped crystals are visible in SEM images of γ-alumina [50] – left, gibbsite – middle and kaolinite - right.

The coordination of surface groups on the γ-alumina surface is slightly more complicated. In addition to singly and doubly coordinated hydroxyls, the γ-alumina mineral contains triply coordinated hydroxyls bound to aluminum atoms in octahedral coordination. The former two groups, however, may also be coordinated to Al atoms in tetrahedral coordination, thus, adding up to five different surface sites in total as explained by the Knözinger and Ratnasamy model, Figure 6 [51].

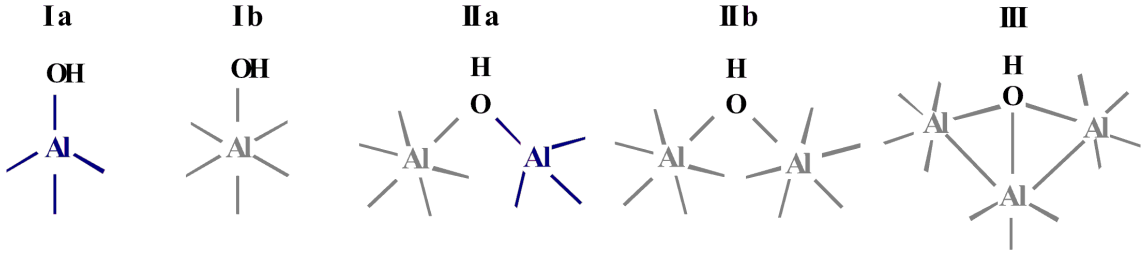

Figure 6: The different hydroxyl groups on γ-alumina (aluminum atoms in tetrahedral coordination in blue, and in octahedral coordination in gray) [51].

The clay mineral kaolinite has a 1:1 layered structure of alternating aluminum hydroxide octahedral and silica tetrahedral sheets that share a common plane of oxygen atoms [52]. The kaolinite surface consists of three morphologically different planes with different chemical compositions: a gibbsite type basal plane, a silica type basal plane and edge planes consisting of the two constituents $Al(OH)_3$ and SiO_2 [40]. According to Zachara et al. [53] and McKinley et al. [54] these hydroxylated sites exhibit acid/base behavior and coordinative properties analogous to those of their component mineral (hydr)oxides [i.e. SiO_2 and $Al(OH)_3$]. Thus, as in the gibbsite case, all OH groups are coordinated to two Al atoms on the gibbsite-like basal plane whereas the tetrahedral siloxane plane consists of

oxygen atoms coordinated to two Si atoms (Si_2O). At the edges a combination of aluminol (Al-OH), silanol (Si-OH) and mixed Al-OH-Si sites can be found.
Trivalent metal ion attachment onto the surface sites discussed above and their reciprocal reactivity is one of the major focal points of this thesis. Thus, trivalent metal ion attachment on mineral surfaces and the spectroscopic speciation methods employed to study the surface reactions at the mineral/water interfaces will be discussed in forthcoming sections.

3.2.2 Trivalent actinide sorption at the mineral surface

Trivalent metal cations can adsorb on mineral surfaces both through inner sphere complex formation and through electrostatic attachment of the positively charged metal cation to a negatively charged mineral surface. In addition, incorporation of the metal can occur either in coprecipitation reactions with the mineral phase in supersaturated solutions or in dissolution and precipitation reactions in saturated solutions resulting in restructuring of an existing mineral phase. Within the framework of the present study precipitation reactions in combination with surface adsorption reactions were found to result in trivalent actinide incorporation on the mineral surface (Article I).

In inner sphere complexation, the mineral surface hydroxyl groups act as σ-donors, which increase the electron density of the coordinated metal ion. Interaction with the Lewis acid i.e. the metal ion, results in strong chemical bonds with usually quite short bond lengths [40]. The trivalent metal can be attached to one or several of the mineral hydroxyl groups in monodentate (Equation 3) or multidentate (e.g. bidentate, Equation 4) complexation, respectively [adapted from 55].

$$\text{S-OH} + \text{An}^{3+} \leftrightarrow \text{S-OAn}^{2+} + \text{H}^{+} \quad (3)$$

$$2\ \text{S-OH} + \text{An}^{3+} \leftrightarrow (\text{S-O})_2\text{An}^{+} + 2\text{H}^{+} \quad (4)$$

As the sorption involves proton dissociation the adsorption reaction is favored at higher pH values, where the surface hydroxyls are deprotonated. The influence of pH on the amount of adsorbed metal ions is generally determined in batch-sorption experiments where the actinide-containing solution is contacted with the mineral phase of interest. By measuring the amount of remaining actinide in solution, the adsorbed amount on the mineral surface can be determined. The pH-dependent sorption can then be expressed in terms of the adsorbed percentage of the trivalent metal ion or the sorption distribution coefficient K_d/logK_d as a function of solution pH, Figure 7. The K_d value is the ratio between the sorbed metal ion concentration and the metal ion concentration in solution given by Equation 5.

$$K_d = \frac{c_0 - c_i}{c_i} \times \frac{V}{m} \quad (5)$$

Here c_0 is the initial metal ion concentration added to the solution in mol/l. The c_i term represents the metal ion concentration remaining in solution after adsorption onto the mineral surface in mol/l. V is the volume of the solution [l] and m is the amount of solid in kilograms.

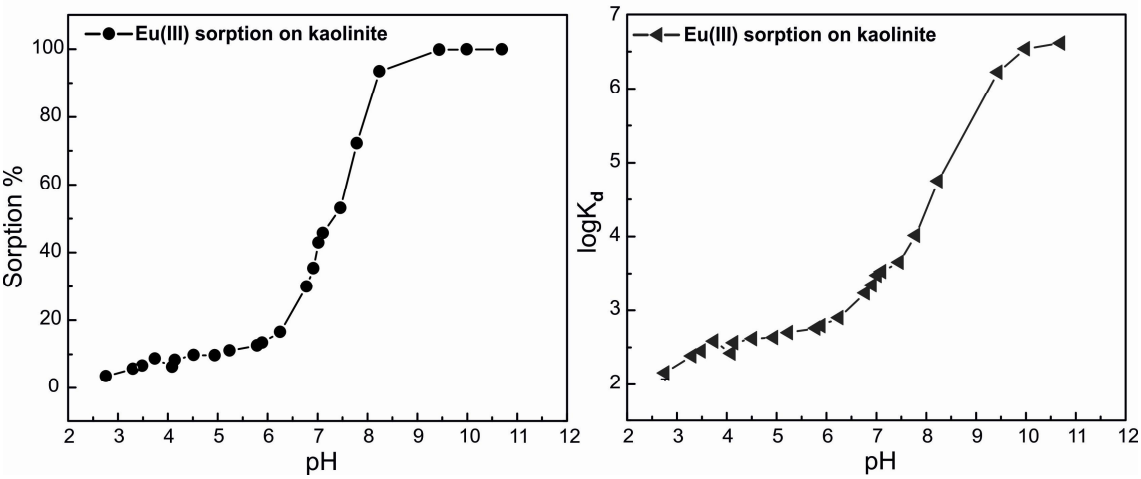

Figure 7: The retention of metals on solid phases can be expressed either as the adsorbed metal ion percentage as a function of pH (left) or as the sorption distribution coefficient K_d or $logK_d$ as a function of pH (right).

Batch sorption investigations are straightforward and provide helpful information about a mineral's sorption capacity, but they do have some drawbacks. The results obtained in batch sorption experiments are highly sample-specific and difficult to extrapolate to different conditions such as varying ionic strengths or redox potentials [56, 57]. Moreover, they provide very little direct information on the sorption mechanisms of the RN involved which in turn does not allow for derivation of the interaction strength between the RN and the mineral surface. In addition, if surface precipitation occurs in the mineral suspensions, the K_d value merely represents the solubility product of the surface precipitate and will not reflect the sorption behavior of the radioelement. Therefore, batch experiments should be complemented by spectroscopic investigations that provide information on the mode of interaction and the direct speciation of the radioelement involved. Speciation techniques employed within the framework of this thesis will be discussed in the following chapter.

The strength of surface complex formation on the surface is tied to the complexation strength of the metal in solution. Radionuclides with low charge, such as the pentavalent actinyl ions, result in lower sorption in comparison to the highly charged tetravalent actinides. As previously mentioned, hydration competes with complexation reactions by ligands as the process of complexation involves the displacement of one or more water molecules by the ligand. This is applicable to surface complexation reactions as well. Thus, surface complexation reactions and solution hydration and complex formation can be considered competing mechanisms. The competition does, however, not exclude the possibility of concurrent sorption through both outer and inner sphere complex formation

as explained by Lee et al. [58], where cations have been found to coexist as inner and outer sphere complexes on muscovite.
When solution reactions and surface complexation reactions combine, ternary metal ion surface complexes form as a result. Attachment of a hydrolyzed metal complex on a mineral surface, results in the formation of a ternary surface/metal-hydroxo species according to Equation 6 [59].

$$S\text{-}OH + An^{3+} + xH_2O \leftrightarrow S\text{-}OAn(OH)_x^{(3-x-1)+} + (x+1)\ H^+ \qquad (6)$$

In the presence of other complexing ligands like silicates or carbonates, ternary surface/metal-silicate and surface/metal-carbonato complexes, respectively, have been identified [45, 60]. The similarity of cation surface-complexation reactions on mineral hydroxyl groups and their hydrolysis reactions in solution has been demonstrated in linear correlations between the surface complexation and the corresponding aqueous phase hydrolysis constants [61, 62]. Such linear free energy relationships have been demonstrated for a multitude of metals on e.g. the clay minerals montmorillonite [63], illite [64] and kaolinite [65].

4 Spectroscopic speciation techniques

For a comprehensive process understanding of the interaction mechanisms between trivalent actinides and the chosen minerals, batch experiments are not sufficient. In this work TRLFS and NMR spectroscopies have been employed to gain information on the underlying mechanisms that govern An^{3+} interactions at the solid/water interface and to get insight into the various surface groups participating in the sorption reactions, respectively.

4.1 Time-resolved laser fluorescence spectroscopy (TRLFS)

Time-resolved laser fluorescence spectroscopy (TRLFS) is a spectroscopic technique with outstanding sensitivity, based on the spontaneous emission of light. Spontaneous emission of light or luminescence describes the process of radiative decay where an excited substance emits electromagnetic radiation upon relaxation. When this relaxation occurs between an excited state and the ground state of same spin multiplicities ($\Delta S = 0$) the luminescence process is referred to as fluorescence. In the case of a transition between levels of different multiplicity ($\Delta S \neq 0$) due to spin exchange in a process referred to as inter system crossing, the term phosphorescence is used instead [66, 67]. Typically, this is correlated with the relaxation time that is longer for phosphorescence than for fluorescence. Some f-elements relax through intense luminescence emission in aqueous suspension. Such actinide and lanthanide fluorophores are Am(III), Cm(III), Bk(III), Cf(III), Pa(IV), U(VI), and Eu(III), Gd(III), Tb(III), respectively. The characteristic optical spectra of these inner transition elements originate from f-f transitions, taking place between the partly filled 4f (lanthanides) and 5f (actinides) energy levels [66, 68-69]. The f-f transitions are sensitive to changes in the ligand field, thus, making TRLFS an extremely useful tool to account for the complex speciation of these elements. In the spectroscopic work performed within the framework of this thesis, the trivalent actinide curium(III) has been used in the majority of the TRLFS investigations. The spectroscopy of this actinide will, thus, be focused on in more detail.

4.1.1 Curium TRLFS

Curium has the electronic configuration $[Rn]5f^7 6d^1 7s^2$. Upon ionization the 6d- and 7s-electrons are lost to form a Cm^{3+} ion with a $[Rn]5f^7$ configuration. In curium(III) TRLFS the luminescence emission between f-states of higher energies to the ground level is monitored. In the curium absorption spectrum, Figure 8 left, particularly three strong f-f transitions from the Z-ground state ($^8S_{7/2}$) to excited states G, H and F can be observed.

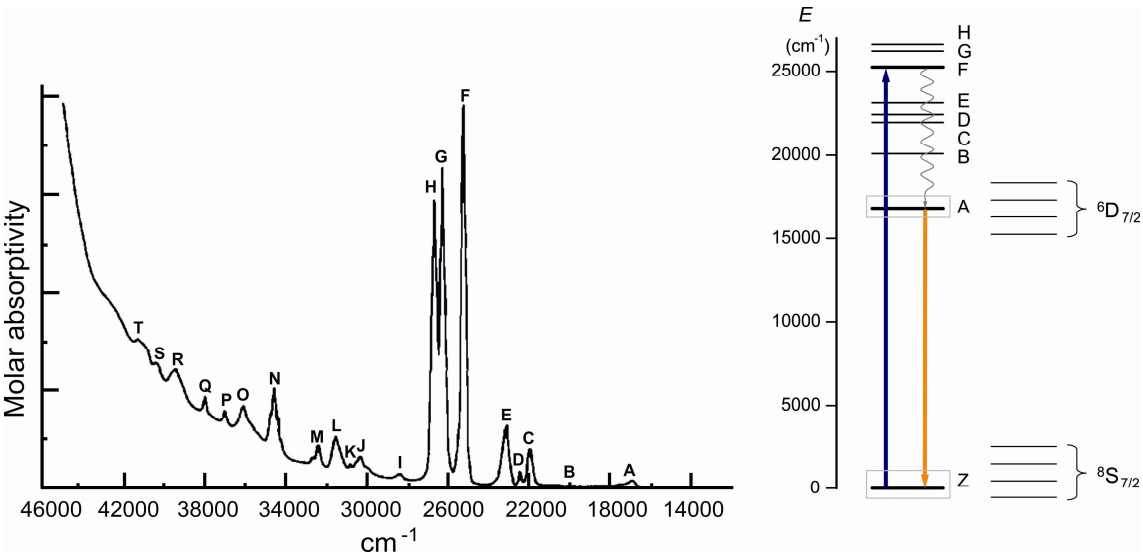

Figure 8: The curium absorption spectrum is characterized by three particularly intense transitions, F, G and H (left). From the excited states radiationless relaxation to the underlying A-state occurs. The fluorescence emission is observed from this A-state to the ground Z-state (right). Figure adapted from [70, 71].

The absorption is followed by nonradiative relaxation to the lower-lying A-state ($^6D_{7/2}$), from which luminescence emission occurs bringing the ion back to the ground state, Figure 8, right. This emission is characterized by an emission spectrum with a peak maximum at 593.8 nm. As the $^6D_{7/2} \rightarrow {}^8S_{7/2}$ transition involves spin exchange the curium ion relaxes through phosphorescence emission even though the luminescence process in most cases is referred to as fluorescence. This convention is also acknowledged in the present work, thus, curium relaxation by emission of electromagnetic radiation will be referred to as either luminescence or fluorescence in the following text.

The excited A-state of the curium ion undergoes a crystal field splitting of about 300 cm^{-1} which is of the same magnitude as the thermal energy of electrons at room temperature (kT = 207 cm^{-1}). This implies that not only the lowest crystal field state is populated at room temperature, leading to a shoulder on the blue side, i.e. at lower wavelengths, of the emission spectrum [68].

The energy of the $^6D_{7/2} \rightarrow {}^8S_{7/2}$ transition is influenced by changes in the ligand field experienced by Cm^{3+}. Thus, inner sphere complexation, where a partial loss of the hydration sphere occurs, results in a shift of the fluorescence emission to higher wavelengths (redshift or bathochromic shift) compared with the spectrum of the aquo ion. Such spectral behavior allows for the direct observation of complexation processes occurring in aqueous suspension. Emission spectra are collected in constant time and wavelength windows by Cm^{3+} excitation with light of constant wavelength. In this study indirect excitation at λ_{ex} = 396.6 nm, taking the curium ion from the ground state to the excited F state, was used. This method will simultaneously excite all present species in the

system and the collected emission spectrum is a superposition of these species. Some experiments were also performed using direct excitation to the emitting energy levels of the A-state, thus, avoiding the nonradiative relaxation process.

More information about the hydration state of the curium ion can be gained from the fluorescence lifetime, i.e. the residence time in the excited state. In aquatic environments f-element spectroscopy is characterized by relatively short fluorescence lifetimes due to the transfer of electronic energy from an excited f-level to the vibrational levels of water molecules in the first coordination sphere of the metal [10, 72, 73]. When some of these quenching entities are lost upon inner sphere surface complexation a longer lifetime is acquired, thus, providing information on the sorption mechanism. If incorporation occurs, the complete hydration sphere is normally lost and the lifetimes become very long. Thus, in most cases inner sphere complexation and incorporation can be distinguished from each other. In outer sphere complexation where the complete hydration sphere remains intact, the distinction between a sorbed outer sphere species and the free aquo ion is difficult. Here, the combination of batch sorption studies where the uptake of the metal ion as a function of pH is obtained can be compared with the TRLFS data. In cases where the collected emission spectrum corresponds to the aquo ion but where the metal ion uptake is significant outer sphere complexation as retention mechanism can be assumed.

In fluorescence lifetime measurements the fluorescence emission is detected as a function of delay time i.e. the time between the laser pulse and the detection by the camera. The received emission spectra at different delay times are then integrated to obtain a decay curve which follows either monoexponential or multiexponential fluorescence decay depending on the fluorescence decay rate (k_{obs}) in relation to the ligand exchange rate and the number of curium species present. If the ligand exchange reaction rate is high compared with the fluorescence decay rate of the excited Cm^{3+} species, an average lifetime of the species and a monoexponential decay is expected. If two or more Cm^{3+} species are present and the ligand exchange rate is low in comparison to the fluorescence decay rate, multiexponential decay follows [74, 75].

For the Cm aquo ion the fluorescence decay rate (k_{obs}) is approximately 15 ms^{-1} corresponding to a fluorescence lifetime (τ) of 68 μs ($k_{obs} = \tau^{-1}$). The fluorescence lifetime values can be linked to the number of hydration water molecules (nH_2O) in the first coordination sphere of Cm(III) using the empirical Kimura equation below [10].

$$n_{H_2O} = 0.65 \times k_{obs} - 0.88 \qquad (7)$$

By substituting the fluorescence decay rate for the curium aquo ion into Equation 7, the number of water molecules surrounding the ion amount to approximately nine.

4.2 Nuclear magnetic resonance spectroscopy (NMR)

Nuclear magnetic resonance (NMR) is a phenomenon that occurs for so called spin active nuclei when they are immersed in a static magnetic field B_0 and exposed to electromagnetic radiation in the radiofrequency (RF) range [76, 77]. Spin active nuclei are those that have unpaired nuclear spin yielding a spin quantum number $I \neq 0$. When these nuclei are exposed to a static magnetic field their magnetic moments (μ) orient themselves with respect to the direction of the magnetic field in 2I+1 ways (Zeeman effect). For nuclei with a spin quantum number of 1/2 such as the proton, which is the most important isotope probed within the framework of this thesis, the number of orientations amount to two: either with the magnetic field or against it, Figure 9 [77].

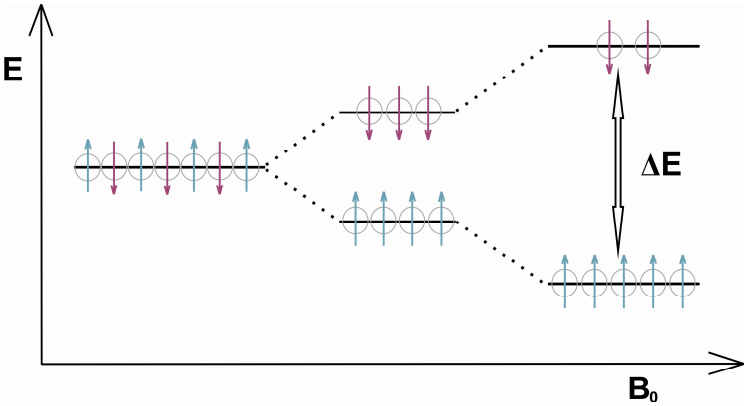

Figure 9: The Zeeman effect for nuclei with a spin quantum number of 1/2: The external magnetic field (B_0) causes the spin active nuclei to orient themselves either with the magnetic field (blue arrows) or against it (red arrows). The energy difference ΔE between the spin states increases as a function of the magnetic field.

The population of the two spin states is given by the Boltzmann distribution in Equation 8.

$$\frac{n_{upper}}{n_{lower}} = e^{-\Delta E/kT} \tag{8}$$

When energy that corresponds to the energy difference between the two spin states is supplied to the spin system, nuclear spins in the lower spin state are excited to the upper one. The excitation energy is supplied to the system as short RF pulses with a frequency (ν) that corresponds to the probed nuclei's resonance frequency, Equation 9 [76].

$$\Delta E = h\nu = \frac{\mu B_0}{I} \tag{9}$$

As the spins return to the lower spin state a small voltage is induced in the coil surrounding the NMR probe. This voltage can be amplified and detected as a function of time, referred to as the free induction decay, FID. The intensity of the signal is proportional to the population difference between the two spin states. Thus, to increase the NMR signal the energy difference ΔE should be increased, which consequently requires

high static magnetic fields. Within this study a magnetic field of 18.8 T, i.e. more than 10^5 times stronger than the magnetic field of the earth, was used throughout the experiments. To obtain the conventional NMR spectrum where the intensity is presented as a function of frequency the FID must be transformed from time domain to frequency domain in a process called Fourier transform (FT), Figure 10. In order for NMR spectra measured at different spectrometers with different magnetic fields to be comparable to each other, the absolute frequency scale is replaced by a dimensionless parameter δ that describes the chemical shifts in terms of the differences in resonance frequencies between the nucleus of interest (ν) and a reference nucleus (ν_{ref}), Equation 10. This quantity is reported in ppm (10^{-6}) of the operating frequency (ν_{spec}).

$$\delta = 10^6 \frac{(\nu - \nu_{ref})}{\nu_{spec}} \tag{10}$$

In ^1H and ^{13}C NMR spectroscopy, the most commonly used reference material is tetramethylsilane (TMS), $Si(CH_3)_4$.

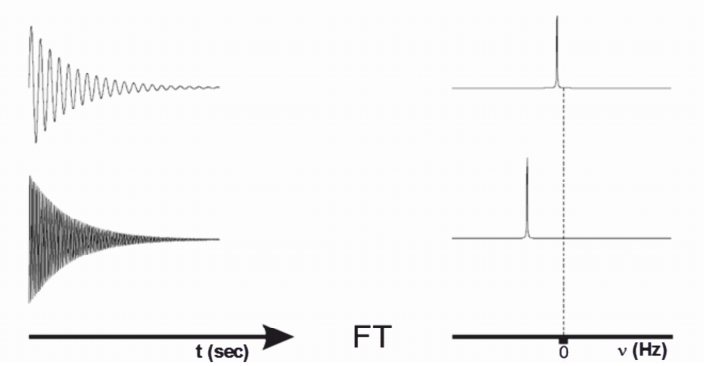

Figure 10: The FID is Fourier transformed from time domain to frequency domain to obtain conventional NMR spectra [78].

4.2.1 NMR of diamagnetic and paramagnetic substances

A magnetic field can induce two kinds of electronic currents in a molecule, diamagnetic and paramagnetic. These two currents flow in opposite directions and give rise to nuclear shielding and deshielding, respectively. The diamagnetic shielding arises from electrons circulating about the direction of the applied magnetic field, thus, inducing a small magnetic field that opposes the externally applied field at the nucleus. This effective field (B) is consequently lower than the applied field by a fraction of σ, referred to as the shielding or screening constant [76].

$$B = B_o (1-\sigma) \tag{11}$$

The electron density in a molecule varies according to the types of nuclei and bonds in the molecule. These variations in the electron densities cause small variations in the magnitude of the opposing field and, therefore, the effective field at each nucleus will vary. This allows for the detection and discrimination of the probed nuclei in different chemical surroundings, known as the chemical shift phenomenon.

When an atom or molecule containing one or more unpaired electrons is placed in a strong static magnetic field, a net magnetization is induced in the substance. This magnetization called paramagnetism produces a new magnetic field that the probed atom or isotope feels in addition to the magnetic field produced by the spectrometer. This induced magnetization causes an isotropic shift of atoms in the vicinity of the paramagnetic substance. Furthermore, paramagnetic substances are very efficient in causing relaxation of the excited nuclear spin states resulting in extremely broad lines potentially to the extent that one is unable to get any NMR signal [79]. Paramagnetic substances are often considered unwanted impurities in NMR investigations [80-83]. However, due to the induced isotropic shifts, they can also provide information on nearest neighbor atoms that are influenced by the paramagnetic substance [84-86]. They are also added to samples to reduce the spin-lattice relaxation times [85, 87].

In this work both diamagnetic (yttrium) and paramagnetic (europium) nuclei were used as analogues for the trivalent actinides in the NMR investigations. Quantitative data could not be obtained from samples containing the paramagnetic europium ion, but the induced signal loss in recorded proton spectra facilitated the detection of surface protons through comparison of recorded NMR spectra with and without the paramagnetic nucleus. Details on these NMR investigations will be provided later in the text.

4.2.2 Solid state NMR

The main aim in the NMR investigations of the present work has been to identify different hydroxyl groups on mineral surfaces, gain information on their quantity and abundance and most importantly their affinity towards trivalent metal ion attachment onto the surface. In the solid-state this cannot be accomplished in a straightforward manner due to the very broad spectral lines caused by the anisotropic couplings in the solid-state which require a different experimental set-up in comparison to conventional solution NMR investigations. The interactions governing solid-state samples and some relevant NMR techniques employed to reduce the influence of these interactions on the measured spectra will briefly be discussed in this section.

Solid-state investigations differ from solution NMR very decisively due to the lack of motion in the solid samples. In solution NMR, spectra consist of a series of very sharp transitions due to averaging of anisotropic NMR interactions by rapid random motions. By contrast, solid-state NMR, where restricted or no internal motion occurs, spectra are very broad. This is due to the multiple orientation-dependent (anisotropic) interactions between the nuclei in the solid [88]. Such interactions are chemical shielding, dipole-dipole

interactions with other nuclei and quadrupolar interactions present for nuclei with spin >½ such as the ^{27}Al nucleus with a spin quantum number of 5/2. These interactions are all dependent on the crystallite orientation with respect to the magnetic field, and as a result, the NMR spectrum of a solid sample contains broad lines, as all the different molecular orientations present in the sample give rise to different spectral frequencies [89].

The dipolar interactions result from the interaction of one nuclear spin with a magnetic field generated by another nuclear spin. The magnitude of this interaction is dependent on the type of nuclei, the inter-nuclear distance and the orientation of the two nuclear spins with respect to the magnetic field. In a strong magnetic field, the orientation of the nuclear spins shows a proportional dependence to $3\cos^2\theta$-1. In solution the molecules reorient quickly so that nuclear spins feel a time average of the spatial part of the dipolar interaction ($3\cos^2\theta$-1) over all orientations and the term averages to zero [90]. A technique referred to as magic-angle spinning (MAS) introduces artificial motion by placing the axis of the sample rotor at the magic angle $\theta = 54.74°$ with respect to B_0. At this angle the term $3\cos^2\theta$-1 is averaged to zero provided that the rate of spinning is fast enough compared to the homonuclear dipolar-coupling linewidth [89]. At spinning rates much less than the dipolar linewidth, little or no effect on the NMR spectrum can be observed. At intermediate spinning rates a manifold of spinning sidebands becomes visible, which are separated by a chemical shift equal to the rate of spinning. For protons with the largest nuclear magnetic moments of spin active nuclei and high isotopic and quantitative abundance in many materials, the homonuclear dipolar coupling linewidth is very large (in some cases more than 100 kHz) [91]. Such spinning frequencies cannot be acquired with conventional equipment and sufficient resolution to allow for structural data is hard to obtain. In the present study spinning speeds of 18 kHz were employed, resulting in rather broad proton spectra with visible spinning sidebands (SSBs). However, by comparing proton spectra with different concentrations of trivalent metals, chemical shift data on various surface hydroxyls could be acquired. This will be explained in more detail later in the text.

To reduce homonuclear dipolar couplings in the sample, one has to increase the distance between interacting nuclei. For this effect, dilution of the probed nuclei can be used. In ^1H NMR investigations of microporous mineral samples, the amount of protons can be reduced by deuterium exchange [92] and by removal of adsorbed water with high temperature calcination of the mineral [93]. The latter method alters the mineral structure through dehydroxylation and was, thus, not employed in this study. Drying treatment is nevertheless important as physisorbed water on the mineral surface will increase the dipolar coupling effects in the spectra.

Another very important interaction in solid-state samples occurs for nuclei with a spin greater than 1/2 with a non-spherical charge distribution. These are known as quadrupolar nuclei. The non-spherical charge distribution can interact with an electric field gradient (EFG) arising from the electric charge distribution in the molecule. This leads to anisotropic linebroadening and sometimes fast relaxation of quadrupolar nuclei, which in turn cause very broad lines in the NMR spectra [76, 94]. Quadrupolar interactions can be

separated into first and second order interactions that are treated separately. Just like the dipolar interactions the first order quadrupolar interaction has an angular dependency of $3\cos^2\theta$-1 with respect to the magnetic field. Thus, with MAS, the first order interaction can be averaged out. The second order interaction also has an angular dependency of two zero points at 30.6° and 70.1°. This interaction cannot be completely averaged out unless the rotor is spun at two angles simultaneously: 54.74° (magic angle) and 30.6° [89]. Within this work the quadrupolar interactions of ^{27}Al in the examined solids, γ-alumina and kaolinite, is rather small and the double rotation was not required to obtain narrow spectra. This low quadrupolar coupling owes partly to the symmetrical electric charge distribution of the tetrahedral and octahedral aluminum units within the mineral structures that consequently lead to low EFG interactions [76, 88, 93].

5 Experimental

A summary and compilation of the experimental set-up including materials, sample preparation and the realization of the macroscopic and spectroscopic investigations will be given in this section. More detailed information of these experiments is found in the Articles (I-V).

5.1 Materials

The minerals chosen for the study are either of synthetic or natural origin. Mineral synthesis, even though time consuming, is beneficial in comparison with using natural minerals as the purity of the end product can be controlled by the use of high grade or ultrapure reagents. In this work, gibbsite (Article I) and one batch of kaolinite (Article II) were synthesized in the laboratory, while the synthetic γ-alumina (Article IV) was purchased and used as received for the experiments. The majority of the kaolinite studies were performed with a natural batch of kaolinite from St. Austell (UK) (Articles II, III, and V).

In the gibbsite synthesis, amorphous $Al(OH)_3$ was precipitated by mixing a 0.33 M $AlCl_3$ solution with 1 M NaOH. The precipitation was carried out in a glove box, under argon atmosphere to eliminate possible contamination by atmospheric carbon dioxide. The formed suspension was transferred into dialysis tubes where dialysis against deionized water (MilliQ) at 70°C for a time span of 4 months was carried out. During the first four weeks of dialysis water exchange was done every day with exception of weekends. For the remainder of the time the water exchange was done 2-3 times per week. The dialysis resulted in a gibbsite suspension with a pH value of 4.2 and a solid content of 41.9 ± 1.0 g/l.

Synthetic kaolinite was obtained by hydrothermal treatment of an aluminosilicate gel at 220°C. Here, a 0.2 M sodium metasilicate ($SiO_2Na_2O{\times}5H_2O$) solution was mixed with 0.2 M aluminum nitrate ($Al(NO_3)_3$) to obtain a white precipitate of $Si_2Al_2O_7$. The gel was separated from the supernatant and dried in an oven at 60 °C over night. 1 g of the dry, finely ground gel and 60 ml MilliQ water were placed in Teflon reactor vessels with outer metal bodies. The reactors were placed in preheated ovens at 220°C for 14 days. Vessels were opened and the intermediate product was separated from the supernatant, dried and crushed. The obtained powder was placed in the reactors with fresh MilliQ water and the pH was adjusted to approximately one with suprapure HCl. The reactors were sealed and kept at 220°C for an additional 10 weeks. After the completed hydrothermal treatment the kaolinite was separated from the supernatant and washed thoroughly with MilliQ water.

All minerals were characterized with multiple methods. N_2-BET analyses were performed to obtain the specific surface area of the mineral particles. SEM-EDX or XPS were used to locate impurities on the mineral surface, while XRD analyses provided information on the phase purity and crystallinity of the materials. SEM or AFM were used to determine the particle size in terms of platelet diameter and height. Results from these characterizations for all minerals are compiled in Table 1.

Table 1: Compiled results from mineral characterizations.

Mineral (ref)	Specific surface area [m^2/g]	Particle size [nm] diameter/height	Elemental composition [atom-%]	Hinckley index
gibbsite (I)	49.5	250±60/16.8±10.4	O – 67.1 % Al – 32.9 % < 1% of Cl and C	-
kaolinite synthetic (II)	22.2	400-1100/200	O - 68.21 ± 2.00 Al - 15.81 ± 0.80 Si - 15.98 ± 1.30	1.01
kaolinite natural (II, 95)	11.7	400-1000/200	O – 68.27 ± 3.40 Al – 15.26 ± 1.50 Si – 16.47 ± 1.90 < 1% of K, Na, Sb, Fe	1.34
γ-alumina (IV)	62.5	-	-	-

5.2 Sample handling

All sample preparation and handling in this study was done under carbonate-free conditions to exclude the influence of carbonate complexation with the trivalent metals and, thus, simplify the interpretation of acquired results. In practice, all work was done in either argon or nitrogen-filled glove boxes where the oxygen content was monitored and kept below 1 ppm throughout sample handling. All solutions brought into the glove box were either flushed with argon or nitrogen or stored in the glove box for weeks prior to the experiments to minimize the carbonate content. A detailed explanation on the sample preparation procedure for the different experiments is given in the respective sections below.

5.3 Batch sorption investigations on Gd^{3+} and Eu^{3+} adsorption onto gibbsite and kaolinite

Batch sorption investigations were mainly conducted in perchlorate media of varying ionic strength, 1-100 mM. Due to radiation safety considerations all batch studies were performed with lanthanide elements, i.e. using gadolinium in the gibbsite studies and europium in the kaolinite studies, respectively. By varying the ionic strength influence of the electrolyte ions on the sorption of the trivalent metal was examined. In outer sphere complexation where electrostatic attachment to the surface occurs, the positive electrolyte cations have been found to compete for sorption sites with tripositive metal ions [44, 96-98]. In investigations where the metal ion concentration was varied over at least one order of magnitude some information on site types (strong vs. weak sites) or saturation properties on the mineral surface could be acquired. If the sorption is independent of the metal ion concentration used, i.e. the position of the pH-edge is constant at a given solid concentration, sorption occurs in the so called ideal sorption range. In this ideal sorption range only one type of surface groups, so called strong sites, participate in the metal ion binding. At higher metal ion loadings deviations from ideal sorption behavior cause a shift of the pH edge to higher pH values. Such non-ideal behavior can result from saturation effects, steric effects, where the attached trivalent metal exerts a repulsive force on metal-ions remaining in solution, or due to heterogeneity of the surface binding sites, i.e. different types of surface sites with different complexation strengths participate in the sorption reaction [99, 100].

The batch samples were prepared in 20 ml polypropylene bottles with sample volumes ranging from 10 to 15 ml. The sorption of gadolinium onto gibbsite (Article I) was investigated in the pH-range 3.5-11.5 in 100 mM $NaClO_4$. A constant gibbsite concentration of 2.2 g/l was used while the gadolinium concentration was adjusted from 6.4×10^{-9} M to 6.4×10^{-5} M. $HClO_4$ or carbonate free NaOH were used for pH adjustments. The batch sorption investigation on europium sorption onto kaolinite (Article II) were conducted in 100 mM $NaClO_4$ using a constant synthetic or natural kaolinite concentration of 0.25 g/l in all samples. The europium concentration was varied between 6.6×10^{-8} M and 6.6×10^{-6} M. The sorption studies were carried out from pH 2 to 11. To investigate the influence of the background electrolyte, additional experiments were performed in 1 mM $NaClO_4$ in the pH range 2.5-12 for the natural kaolinite mineral (unpublished). The solid concentration was kept at 0.25 g/l but the europium concentration was varied between 2×10^{-7}-2×10^{-6} M. Samples for all batch investigations were allowed to equilibrate for at least three days after metal ion additions and pH adjustments. After the equilibration time the samples were pipetted in bottles for ultracentrifugation inside the glove box or the centrifugation was done at lower speeds directly in the 20 ml polypropylene bottles used in the batch sorption experiments. The gibbsite samples could be separated at lower speeds, 18000 rpm, while the clay minerals required ultracentrifugation speeds of 60-90000 rpm. The adsorbed amount of gadolinium or europium onto the minerals was determined from the separated supernatant solutions using ICP-MS. The dissolved concentrations of the mineral components, either Al in case of gibbsite or Al and Si in case of kaolinite, were analyzed simultaneously from each sample. As previously

mentioned, batch investigations provide very limited information on the underlying sorption mechanism. Therefore, acquired batch sorption data must be complemented with spectroscopic investigations that provide information on the metal ion speciation in the system.

5.4 TRLFS investigations on Cm^{3+} adsorption onto gibbsite and kaolinite

5.4.1 TRLFS samples

TRLFS investigations in Articles I and II were performed in 100 mM $NaClO_4$, while 1 mM background electrolyte concentrations were used in the experiments of Article III. The curium concentration and mineral content were kept constant at 2×10^{-7} M and 0.5 g/l (gibbsite) or 0.25 g/l (kaolinite), respectively, in each sample. The trivalent actinide was obtained from an acidic curium stock solution (2×10^{-5} mol/l in 100 mM $HClO_4$) with an isotopic composition of 97.2% ^{248}Cm, 2.8% ^{246}Cm, and < 0.01% ^{244}Cm. Each sample with a volume between 5 and 10 ml were equilibrated at least two days before TRLFS experiments unless otherwise stated. The sample equilibrium pH was measured before each spectroscopic experiment after which 3 ml of the sample was pipetted into quartz cuvettes. To prevent air and more importantly carbonate contamination upon removal from the glove box for the TRLFS measurements, the cuvettes were sealed with a cap and parafilm. After completed measurements the samples were brought back into the glove box, combined with the remainder of the suspensions, and the sample pH was again adjusted in steps of 0.3-0.5 pH-units. Thus, the complete studied pH-range (pH ~ 5-12 in gibbsite experiments and 3-13 in kaolinite experiments) could be covered with the use of three to five parallel samples.

5.4.2 Experimental set-up

The TRLFS measurements were done with a combined laser system of a solid state Nd:YAG laser and a dye laser. The dye, Exalite 398, with an intensity maximum at 398 nm, was chosen for the dye laser. In Articles I and II, curium(III) excitation at λ_{ex} = 396.6 nm was done with a tunable dye laser (Continum, Powerlite 9030, ND 6000), pumped by a Nd:YAG laser at 10 Hz. The laser pulse energy, controlled by a photodiode, was between 2.5 and 3.5 mJ in all measurements. The fluorescence emission was detected with an optical multichannel analyzer consisting of a polychromator (Chromex 250) with a grating of 300, 600 and 1200 lines/mm respectively and an ICCD camera. The emission spectra were recorded in the range 580-620 nm, 1 μs after the exciting laser pulse in a time window of 1 ms. To record the fluorescence lifetime the delay time between the laser pulse and the registering by the camera, in a constant time window of 1 ms, was varied between 1 μs and 1200 μs. In Article III the spectroscopic study was performed with a

pulsed Nd:YAG (Continuum Surelite) pumped dye laser set-up (Radiant dyes Narrow Scan). The emitted fluorescence emission light was directed into a monochromator (SR303i, Andor) with a 1200 lines/mm grating and a wavelength range of 580-620 nm. The emission was monitored with a CCD camera (iStar, Andor) 1 μs after the exciting laser pulse in a time window of 10 ms. Fluorescence lifetime measurements were done in delay steps of 10-25 μs up to 850 μs delay times. The laser pulse energy was kept constant between 4-6 mJ in all experiments.

5.4.3 Data analysis and interpretation

As briefly mentioned the curium spectroscopy was performed by indirectly exciting the ion and, consequently all present species to the excited F-state and monitoring the fluorescence emission of the species from the lower-lying A-state back to the ground level (Figure 8, right). Thus, the emission spectra acquired as a function of mineral suspension pH represent the average spectra of all curium species present. In order to acquire knowledge about the single species, their relative distributions and their hydration state, emission spectra have to be deconvoluted. In combination with the lifetime data, conclusions can then be drawn on the surface complex structures and the sorption mechanism in the mineral environment at any given pH value.

In the deconvolution procedure the well-known emission of the Cm aquo ion serves as a reference, and it is subtracted from the spectra which show contributions from the emission of the first sorption species at lower pH-values. At the lowest pH-values only a slight deviation from the aquo ion spectra is obvious and appears as a small shoulder at higher wavelength which increases with increasing pH and, consequently, illustrates the increasing contribution of the first sorbed species in the samples. The obtained difference spectrum, thus, is a pure spectrum of the first adsorbed species, assuming that no other species are present in the system under the given conditions. This process can then be extended using the spectrum of the aquo ion and the first adsorption species to isolate the pure spectrum of the second sorption species, and so forth for all species in the system.

This deconvolution procedure was carried out with the OriginLab Origin data analysis software. Considering all pure component spectra of the system, the relative distributions of involved species can be obtained with any spreadsheet program by the least-squares fitting method where values (fractions of individual species) that yield the lowest sum of squares (square of residual spectrum) are sought for. In this study, Excel was used for all calculations. Once the relative species distribution based on measured fluorescence intensities has been obtained, all values must be corrected with fluorescence intensity (FI) factors that account for variations e.g. in the molar absorptivity at the excitation wavelength and the fluorescence quantum yield of the species involved. FI-factors can be determined considering the measured integrated fluorescence intensity with respect to the excitation energy of the laser system using the same least squares fitting method. By taking into account the FI factors an accurate species distribution can be calculated.

To obtain fluorescence lifetime decay curves, the curium emission is monitored as a function of delay time. The set of emission spectra are thereafter integrated to acquire the fluorescence intensity. By plotting the natural logarithm of the fluorescence intensity as a function of delay time, the decay curves are obtained. These are fitted either linearly or biexponentially, depending on the number of curium species present. When more than two species contribute to the fluorescence signal the fitting procedure becomes difficult. A correct fitting would require an exponential fit of third or higher order involving at least six parameters to fit simultaneously. This easily results in overparameterization of data and consequently to very big uncertainties of the received fluorescence lifetimes.

5.5 NMR investigation on Y^{3+} and Eu^{3+} adsorption onto γ-alumina and kaolinite

5.5.1 NMR samples

The NMR samples were prepared in a glove box just as all the batch and TRLFS samples. However, after mineral separation the samples were open to air until final drying treatments before the NMR measurements. Both γ-alumina and kaolinite samples were prepared in HDPE-bottles at a constant pH of 8.0. The paramagnetic lanthanide europium and the diamagnetic transition metal yttrium were used instead of trivalent actinides in the experiments.

Samples were prepared by suspending the solid in either MilliQ water (γ-alumina, Article IV) or 1 mM $NaClO_4$ (kaolinite, Article V) and introducing the trivalent metals in varying concentrations. In the γ-alumina study two sets of samples were prepared without metal ion addition at four different pH values: 4, 6, 8, and 10 to attain information on pH effects on the ^1H NMR spectra. Sample pH adjustments were carried out daily until a stable pH close to 8.0 was obtained (or pH 4, 6, 8, and 10 in γ-alumina samples without metal ion addition). The samples were allowed to equilibrate for at least six days before they were separated by centrifugation at 20000 rpm. An aliquot of each metal ion containing sample was separated at 80000 rpm for ICP-MS analysis of Y^{3+} and Eu^{3+} concentrations remaining in solution in order to extract their adsorbed amounts on the mineral surface. The recovered solid was dried in an oven at 55°C over night. The solid to liquid ratio was 4g/l, with europium and yttrium concentration of 6.58×10^{-8}-1.32×10^{-4} and 6.58×10^{-7}-3.95×10^{-4} M, respectively, in the γ-alumina samples. In the kaolinite samples 5 g/l of solid and 4×10^{-6}-8×10^{-5} M Eu^{3+} and Y^{3+} were used. Before NMR experiments the samples were dried in a vacuum oven (Vacuum Systems, Finland). To eliminate physisorbed water from the mineral, all samples were heated using a ramp temperature of 1°/min, with the following specific drying conditions: 110°C, 5 h, 20 mTorr (γ-alumina europium samples), 150 °C, 48 h, 20 mTorr (γ-alumina yttrium samples) or 180°C, 5h, 0.2 mTorr (kaolinite samples). The dried samples were sealed under vacuum and transferred into a N_2-glove box where the oxygen and moisture contents were monitored to be less

than 1 ppm throughout the sample handling, thus, assuring that samples were not rehydrated before NMR measurements.

5.5.2 Experimental set-up

Both the γ-alumina ^{1}H as well as the kaolinite ^{1}H and ^{27}Al single-pulse MAS NMR experiments were performed on a Bruker BioSpin Avance III NMR spectrometer using a Bruker triple-resonance MAS probehead. 3.2 mm zirconia rotors were filled in the N_2-glove box with the dried mineral samples. Kel-F® (polychlorotrifluoroethylene) caps were used to seal the rotors and some Kel-F® oil was spread between the cap and the rotor wall to ensure air tightness of the rotors after removal from the glove box. Parameters used in the experiments for the two nuclei, ^{1}H and ^{27}Al, are compiled in Table 2.

Table 2. Parameters used in the NMR experiments.

	Resonance frequency (MHz)	Magnetic field (T)	Exciting pulse	Relaxation delay (sec)	No. of scans	Chemical shift reference
^{1}H	800.13	18.8 T	90°(3.7μs)	40	160	adamantane, $C_{10}H_{16}$*
^{27}Al	208.49	18.8 T	10°(0.5μs)	2	240	alum, $KAl(SO_4)_2 \times 12H_2O$**

** chemical shifts given relative to tetramethylsilane (TMS)*

*** chemical shifts given relative to alum, which itself is -0.35 ppm relative to 3 M $Al(NO_3)_3$ at the magnetic field 18.8 T.*

Solid adamantane and alum were used as secondary references because of easier handling in comparison to the liquid standards TMS and $Al(NO_3)_3$. All the samples were spun with dry air at 18.0 kHz. In the kaolinite study the spinning-speed was stabilized by a Bruker MAS controller +/- 1 Hz.

5.5.3 Data analysis and interpretation

Both γ-alumina and kaolinite samples were measured in two turns so that the europium-containing and yttrium-containing samples were measured separately. The series of samples that were directly compared with one another were dried together under identical conditions and the experimental set-up in terms of magic angle adjustment and shimming (controlling the homogeneity of the magnetic field) was kept constant. The tuning and matching of the probehead to the transmitter frequency was done separately for all samples. After the measurements, phase, background, and baseline corrections were done for all collected spectra. At first, zero-order and first-order phase corrections had to be done due to errors induced by FT of the FID. The first order phase is a frequency dependent phase that arises from the delay between the pulse and acquisition [101]. In this

study the first order phase was acquired from the measured reference material i.e. adamantane or alum for ^{1}H and ^{27}Al spectra, respectively, and the same phase parameter was used for all measured mineral samples. Zero order phase correction is frequency independent and arises from small phase differences between the receiver and the signal [101]. This correction was done manually by adjusting the phase a few degrees for each sample spectrum. The aim was to get the proton peak and the center transition in the aluminum spectra to have the precise same shape and phase with one another to allow for direct comparison of the spectra. In some cases a perfect match between all spectra in one series could not be acquired due to the multiple spectral corrections involved. These spectra were not considered for data interpretations.

The background correction was done by subtracting the ^{1}H MAS NMR spectrum of the empty rotor from the sample spectra. The aluminum background correction was not needed. The baseline must be corrected to yield a flat baseline so that no errors upon integration of the spectra are introduced. The integrals are used to acquire quantitative data on the number of protons and aluminum atoms in the sample. The proton spectra were corrected using the cubic spline function in the 80-(-80) ppm region. Approximately 10-14 points were selected as true baseline points for the spline correction. The ^{27}Al spectra on the other hand were corrected using a 5th grade polynomial which was manually fitted to the baseline. Finally, for a direct comparison of spectra that were acquired from slightly different sample amounts (rotorfilling will vary to some extent) data were normalized. The γ-alumina spectra (Article IV) were normalized to the same mass (determined by gravimetry). This method, however, was not satisfactory due to the limitations of the analytical scale in the kaolinite study (Article V) where the trivalent metal only removed a very small portion of the total proton signal. Small errors in mass had a large influence on the proton spectra. Therefore, proton spectra acquired from the kaolinite samples were normalized with respect to the amount of aluminum in the samples, assuming that the aluminum concentration per unit mass is constant in all samples. By integrating the aluminum spectra and setting one sample integral to 100% and comparing the other integrals with this sample, normalization factors were acquired that were further used to normalize the proton spectra. Normalized spectra could thereafter be compared with one another to acquire information on the different surface protons, i.e. hydroxyl groups on the mineral surfaces. Information on exchanged protons due to trivalent metal ion attachment to the surface could also be obtained.

6 Results and discussion

6.1 Batch and TRLFS results on Gd^{3+} and Cm^{3+} adsorption onto gibbsite (Article I and unpublished data)

The adsorbed fraction of gadolinium on the gibbsite surface vs. pH showed a strong increase over a narrow pH range, Figure 11. The resulting pH edges were found to be congruent for gadolinium concentrations between 6.4×10^{-9} and 6.4×10^{-7} M indicating that sorption occurs in the so called ideal sorption range as explained in the previous chapter. Uptake starts above pH 5 and is complete at around pH 7.5. At the two higher metal ion concentrations, 6.4×10^{-6} and 6.4×10^{-5} M, a shift of the pH curve to higher pH values occurs and close to complete sorption is attained at pH 8.5.

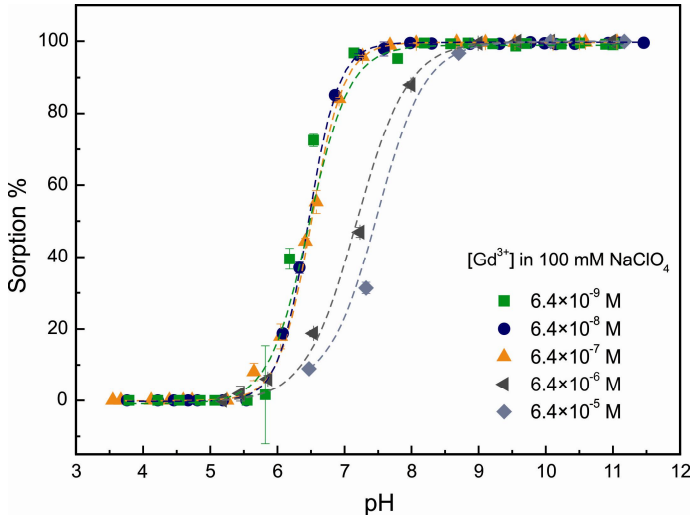

Figure 11: Gd^{3+} retention onto gibbsite as a function of suspension pH. The metal ion concentration was varied between 6.4×10^{-9} and 6.4×10^{-5} M, while the solid concentration and ionic strength were kept constant at 2.2 g/l and 100 mM, respectively.

In Figure 12 left, selected curium emission spectra below pH 6 are presented. They can all be seen to deviate slightly from the spectrum of the pure aquo ion (black curve) indicating a change in the hydration state of the curium aquo ion. These results imply that the attachment mode of the trivalent metal occurs mainly through the formation of a chemical bond between the metal ion and the mineral surface and outer sphere attachment can be neglected. This conclusion is reasonable with respect to the relatively high isoelectric point of the gibbsite mineral at pH 11.0, which indicates the predominance of protonated surface functional groups (formation of $Al–OH_2^+$) over a wide pH range, inducing a

positive surface charge. Thus, no electrostatic interaction between the gibbsite surface and metal cations should take place at pH below 11. In Figure 12 right, selected emission spectra over the whole investigated pH range are shown.

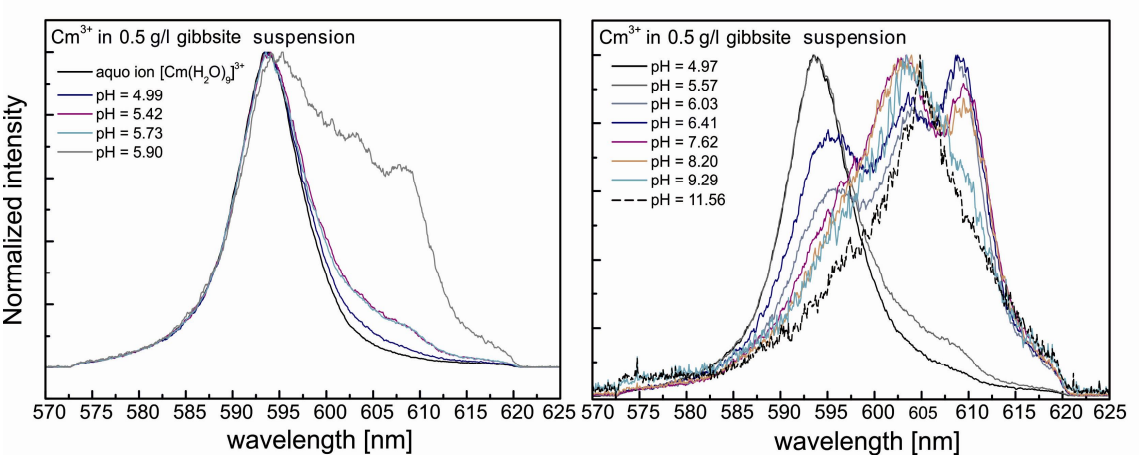

Figure 12: Selected curium emission spectra left) below pH 6, right) over the complete investigated pH range 5-11.56.

The spectra do not show a steady evolution with increasing pH, but the presence of the three visible peaks at 593.8 nm, 603-604 nm, and 609-610 nm vary slightly in intensity independently of pH. As an example the emission spectrum at pH 6.03 has a lower contribution of the peak at 593.8 nm than the spectrum at pH 6.41.

The aquo ion is responsible for the peak at 593.8 nm as discussed in Section 4.1.1. At pH $\geq$ 6.4, the spectrum shows additional peak maxima at 603-604 and 609-610 nm. Above pH 8.2 the peak of the aquo ion disappears as the majority of the trivalent actinide is adsorbed on the gibbsite surface. The peak at 609-610 nm can be seen to level off with increasing pH until it is completely disappeared at pH 11.56. This incongruent behavior of the emission peak appearing when the pH is increased towards the neutral pH range and then slowly disappearing towards the alkaline pH range could be assigned to arise from curium incorporation at the gibbsite surface in a series of experiments where the gibbsite suspension was deliberately oversaturated with respect to aluminum. In these oversaturation experiments a solid sample of gibbsite was suspended and equilibrated in aqueous solution at a near neutral pH (pH = 6.8) and curium was added to the suspension. After 15 days the emission spectrum was recorded and found to consist of one single peak in contrast to what was observed when the sample pH was increased in small steps from acidic pH towards the neutral pH region. Upon addition of 10^{-4} M aluminum to this gibbsite suspension the slow development of a peak at approximately 609 nm could be observed in the emission spectra measured 0-4 d after the aluminum addition, Figure 13 left. This spectral behavior can be understood when considering the solubility behavior of gibbsite as a function of pH, Figure 13 right, as discussed below.

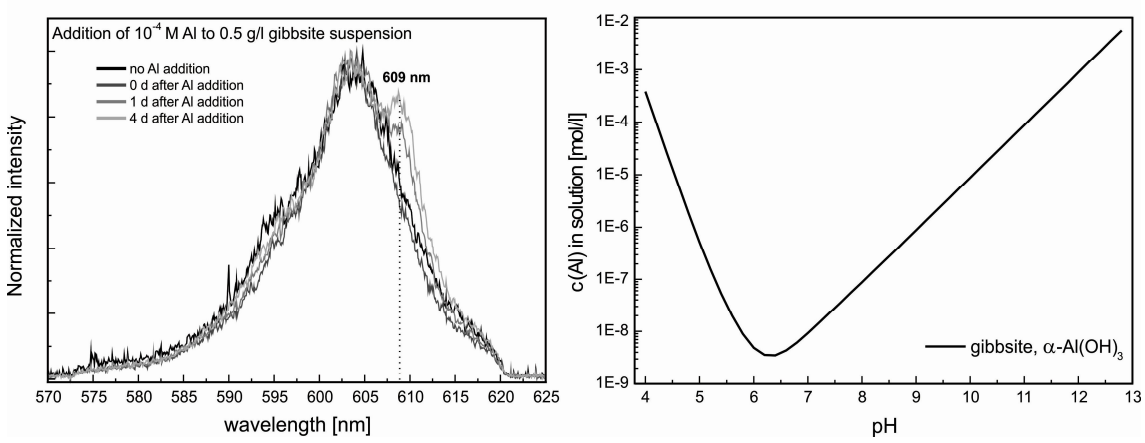

Figure 13: Left - Curium emission spectra after addition of 10^{-4} M aluminum to gibbsite suspensions at pH 6.8. Right - Gibbsite solubility curve as a function of pH.

The TRLFS studies were conducted using sample series with originally low pH, as both the gibbsite stock suspension (pH 4.2) as well as the added curium solution (in 0.1 M $HClO_4$) were acidic. As Figure 12 shows, gibbsite solubility decreases when moving from the acidic pH range towards the solubility minimum at pH 6.3. Thereafter the solubility increases again in the alkaline pH range as a consequence of the formation of anionic aluminate species. The spectroscopic investigations were, thus, always performed by initially increasing the pH into a region of lower Al solubility. At pH above 8.2 where the intensity of the 609-610 nm peak starts diminishing as a function of increasing pH, gibbsite solubility can be seen to increase by close to three orders of magnitude from 10^{-7} M at pH 8 to 10^{-4} M at pH 11. The fact that the curium species at 609-610 nm appears in a pH region ranging from 6 to 8.2 and then decreases again points to the existence of an incorporation of curium at the gibbsite surface as a result of dissolution and re-precipitation of the mineral. The oversaturation results described above also reveal that this incorporated species does not form instantaneously but its formation proceeds over a time period of several days. This can explain the intensity variations of the visible peaks in the emission spectra with increasing pH.

Peak deconvolution as explained above to extract pure component species, was not straight forward due to this very inconsistent presence of various species. The derived emission spectra of the single species in the gibbsite suspension are presented in Figure 14 but their relative distributions could not be obtained due to the fluctuating presence of the aquo ion, one or two surface complexes and the incorporated species that did not allow for extraction of fluorescence intensity (FI) factors necessary for an accurate species distribution. The light gray emission spectrum of species 1a is approximated from only a few emission spectra in the acidic pH range and the existence of this species cannot be verified. The two other species, species 1b (blue spectrum) and species 2 on the other hand have been confirmed in several emission spectra in the gibbsite environment. These can be ascribed with high certainty to two curium inner sphere complexes on the gibbsite surface.

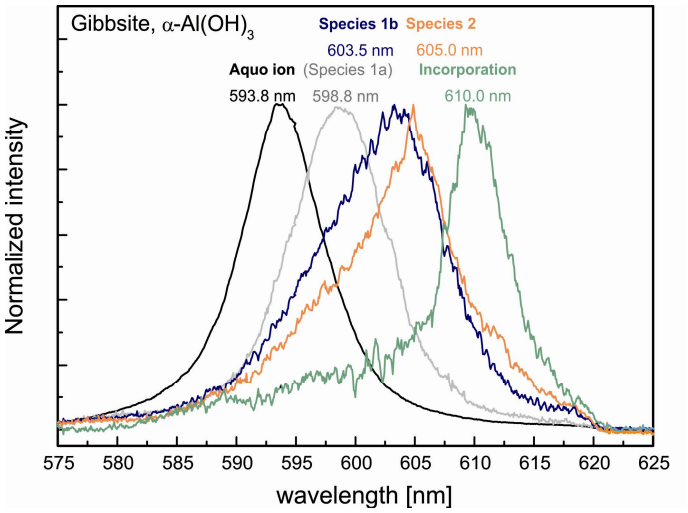

Figure 14: Pure component spectra for curium in gibbsite suspensions derived by deconvolution of sum spectra presented in Figure 12.

Obtained lifetimes for the surface complexes lie in the range of 140-150 µs, which corresponds to on average 3.5–3.8 H_2O entities left in the first hydration sphere of the curium ion according to Equation 7. The incorporated species has a slightly longer lifetime of 180-200 µs, implying that this species is still surrounded by 2.4–2.7 water molecules. However, it is not evident to which extent the hydroxide ions in the gibbsite crystal structure contribute to fluorescence quenching. Thus, more exact data on the nature of this incorporation species and its hydration state cannot be provided. Nevertheless, the presence of this species is clear proof that mineral surfaces cannot be considered as 'inert' with regard to chemical variations as done in many studies. In the batch sorption investigations no evidence pointing towards incorporation could be acquired, thus, emphasizing the importance of spectroscopic investigations to provide molecular scale information on the retention mechanisms occurring at the solid/water interface.

6.2 Batch and TRLFS results on Eu^{3+} and Cm^{3+} adsorption onto kaolinite (Articles II, III and unpublished data)

The pH-dependent fraction of adsorbed europium on both synthetic and natural kaolinite results in pH edges with similar pH edge positions for europium(III) concentrations of 6.6×10^{-8} M and 6.6×10^{-7} M in 100 mM $NaClO_4$. When the metal ion concentration is increased to 6.6×10^{-6} M, deviation from the ideal sorption range resulting in a shift of the pH-edge position is observed, Figure 15.

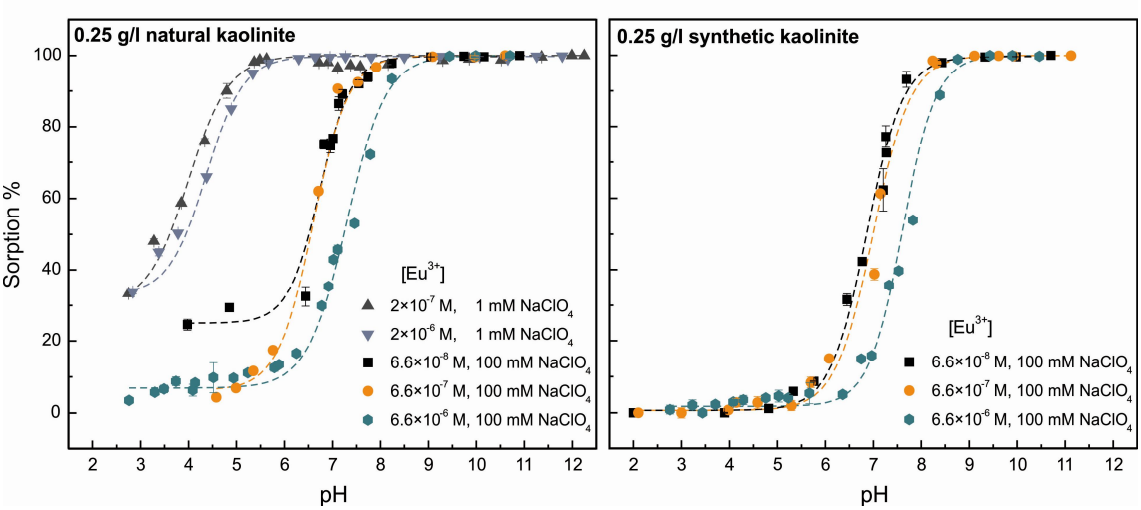

Figure 15: Eu^{3+} retention onto natural kaolinite (left) and synthetic kaolinite (right) as a function of suspension pH in varying metal ion concentrations and ionic strengths.

Differences in europium uptake between the synthetic and natural mineral could be observed mainly for the lowest Eu^{3+} concentration of 6.6×10^{-8} M. In contrast to the synthetic kaolinite where no Eu^{3+} sorption could be detected below pH 5, Eu^{3+} sorption was found to be noticeable even below pH 4 for the natural kaolinite. This difference may arise from greater Eu^{3+} retention through electrostatic attachment on the permanent negative charges of the natural kaolinite mineral which is not the case for the purer synthetic product. Small amounts of impurities of lower valence than aluminum(III) or silicon(IV) such as Fe(II)/Fe(III)/Sb(III) (Fe and Sb impurities were found in the natural kaolinite mineral) as well as isomorphic substitution of Si(IV) by Al(III) in the mineral's siloxane layer are known to induce a permanent negative charge on the mineral surface that favors the electrostatic attachment of cations (e.g. 40, 102). A higher negative charge of the natural kaolinite in comparison with the synthetic product was found in ζ-potential measurements, thus, affirming outer sphere complexation as the reason for the increased uptake in the natural kaolinite suspension at pH < 5.

When reducing the ionic strength from 100 mM to 1 mM and consequently the competition of electrolyte cations for the negative sorption sites on the kaolinite surface, a substantial increase in europium uptake can be observed at pH values below 7, Figure 15. Similar large effects due to variations in ionic strength on metal ion sorption on kaolinite have been reported [103, 104]. Explanations provided for the large differences observed are not solely based on the reduced competition between electrolyte cations and the investigated metal ion for negative sites at the mineral surface but they are related to ion pair formation or coulombic interactions between the charged surface and the sorbing ions. In Ni^{2+} sorption studies on kaolinite the decreased nickel sorption when increasing the ionic strength was attributed to changes in the nickel activity and the formation of nickel-electrolyte anion ion pairs [103]. Due to the increasing amount of ion pair formation in more concentrated electrolytes the free Ni^{2+} concentration is reduced in the

equilibrating solution. This ion pair effect was demonstrated in NO_3^- and SO_4^{2-} electrolytes where the latter anion has a greater tendency towards ion pair formation with Ni^{2+}. A substantial decrease of Ni^{2+} uptake on kaolinite in the sulfate background was indeed observed in comparison to nitrate environments indicating that ion pair formation can have a great influence on the sorbed quantity of the metal ion.

The perchlorate anion is considered a weak ligand and ion pair formation between Eu^{3+} and ClO_4^- in the 1 and 100 mM electrolyte concentrations used in our experiments should not be very pronounced. Ion pair formation, however, has been observed between the trivalent indium cation and perchlorate ($In(ClO_4)(H_2O)_5^{2+}$) in EXAFS studies [105]. Thus, ion pair formation as a reason for the observed differences in Eu^{3+} uptake in the two perchlorate concentrations cannot be ruled out.

In a study on Cr^{3+} sorption by kaolinite, the differences observed in the sorption properties with increasing ionic strength was attributed to a reduction of the attractive force between the negative electrostatic potential on the mineral surface and the inner sphere adsorbing metal cation as the negative electrostatic potential is decreased by increasing the ionic strength [104]. In other words, the coulomb attraction does not solely affect the outer sphere sorption of positive ions on a negative surface but the reduced negative potential also has an influence on the amount of inner sphere sorbed cations.

The underlying mechanism for the increased Eu^{3+} retention at low ionic strength in our experiments could only be deduced from TRLFS investigations. Emission spectra and fluorescence lifetimes were collected in 100 mM $NaClO_4$ for both synthetic and natural kaolinite suspensions over a broad pH range of 3-13 (Article II). Curium speciation in the natural kaolinite environment was further investigated at lower ionic strength (1 mM) over the pH range 3-12 (Article III). Obtained pure component spectra, derived by deconvolution of sum spectra, and corresponding species distributions at the lower ionic strength are presented in Figure 16.

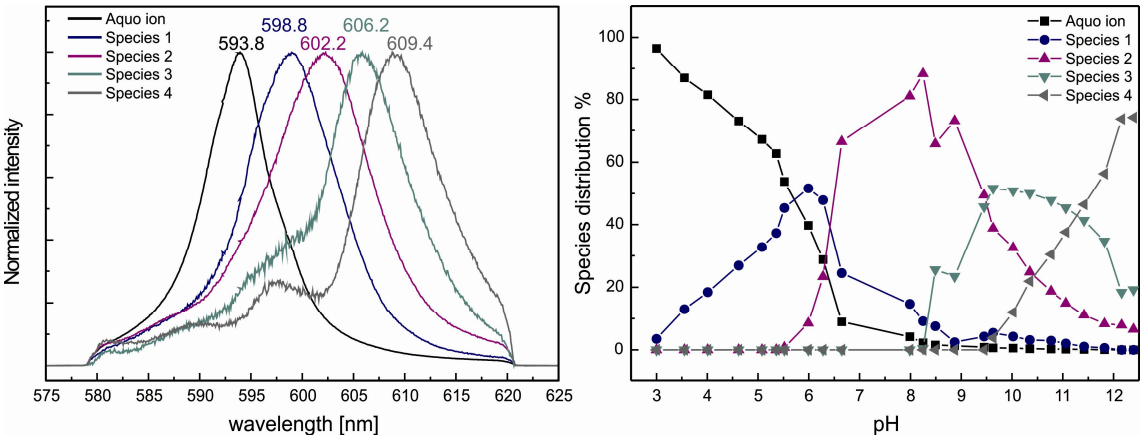

Figure 16: Pure component spectra and the corresponding species distribution of Cm(III) sorption onto natural kaolinite in 1 mM $NaClO_4$ derived by deconvolution of sum spectra.

From the batch studies on 2×10^{-7} M Eu^{3+} sorption onto the natural kaolinite mineral in 1 mM $NaClO_4$ (Figure 15) approximately 30% of the metal ion can be seen to attach to the mineral surface at pH 3. At this pH nearly 100% of the acquired fluorescence emission spectrum corresponds to the curium aquo ion. As previously mentioned outer sphere complexation cannot be distinguished spectroscopically from the dissolved curium aquo ion as both the aqueous and the surface species retains the full hydration sphere. Thus, the ligand field affecting the crystal field states of the curium ion remains unchanged leading to identical emission spectra for both species. Based on the batch investigations the aquo ion spectrum at pH 3 corresponds to both outer sphere curium complexes on the kaolinite surface (30%) and the curium aquo ion in solution (70%).

Above pH 3 the amount of the first inner sphere surface complex (peak maximum at 598.8 nm) increases and at pH 5.5 half of the curium speciation is comprised of this surface complex. In the batch study at 1 mM $NaClO_4$ close to 100% of the europium ion is adsorbed at this pH which would imply that the other half of the species present in the kaolinite suspension belongs to the outer sphere complex. In sorption investigations in 100 mM $NaClO_4$ the Eu^{3+} retention at 6.6×10^{-7} M concentrations is close to zero below pH 5 i.e. neither outer sphere nor inner sphere sorption occurs in this acidic pH range. This means that both electrostatic attachment and the amount of inner sphere complexes have indeed been increased in the lower ionic strength. Above pH 8, no aquo ion can be measured anymore implying that inner sphere complexation becomes the sole mode of attachment in the kaolinite environment. From the deconvoluted emission spectra above, a total of four inner sphere complexes were obtained. Thus, trivalent metal ion speciation in 1 mM electrolyte concentrations over the pH range 3-12 can be explained by the formation of one outer sphere and four inner sphere complexes on the natural kaolinite mineral surface. The number of inner sphere complexes in the 100 mM background electrolyte concentration also amounts to four in both synthetic and natural kaolinite environments.

Lifetimes were collected in both studies over the complete pH range. It has to be pointed out, however, that some of the lifetimes in the study conducted in 100 mM $NaClO_4$ background were obtained from so-called wet paste samples measured at temperatures below 20 K because data obtained from kaolinite suspensions at room temperature was too scattered. Lifetimes obtained in 1 mM $NaClO_4$ could be acquired directly from the kaolinite suspensions due to the superior fluorescence intensities owing to the use of a different laser set-up than in the experiments conducted at higher background electrolyte concentrations. Thus, only these lifetimes will be discussed below. Obtained lifetimes for the inner sphere complexes lie between 116 ± 13 μs (below pH 9.3) which corresponds to on average 4.7 H_2O entities left in the first hydration sphere and 132 ± 5 μs (above pH 9.3) yielding approximately 4.0 H_2O. Assuming that the OH^- ligand quenches the fluorescence emission to a lesser extent than H_2O does [106], the three first inner sphere complexes with peak maxima at 598.8, 602.2, and 606.2 nm were assigned to $>Cm(H_2O)_5^{2+}$, $>Cm(OH)(H_2O)_4^{+}$ and $>Cm(OH)_2(H_2O)_3$ on the kaolinite surface. The fourth curium inner sphere complex could not be assigned to $>Cm(OH)_3(H_2O)_2^-$ arising from further hydrolysis of surface-bound curium according to solution speciation calculations using the PhreeqC code [20]. Instead oversaturation experiments, where excess amounts of

aluminum, silicon, or a combination of both were added to alkaline kaolinite suspensions, indicated that interaction of curium with dissolved/colloidal silicates that form in solution upon kaolinite mineral dissolution occurs in the kaolinite environment. The formation of colloidal silicates could, however, be excluded in experiments where silicon was added to curium suspensions without the mineral phase, thus, confirming the formation of a ternary kaolinite/curium/silicate complex on the kaolinite surface. The curium emission spectra and fluorescence lifetimes acquired upon silicon addition to the kaolinite suspension are presented in Figure 17 together with the emission spectra obtained from pure kaolinite suspensions upon increasing the suspension pH.

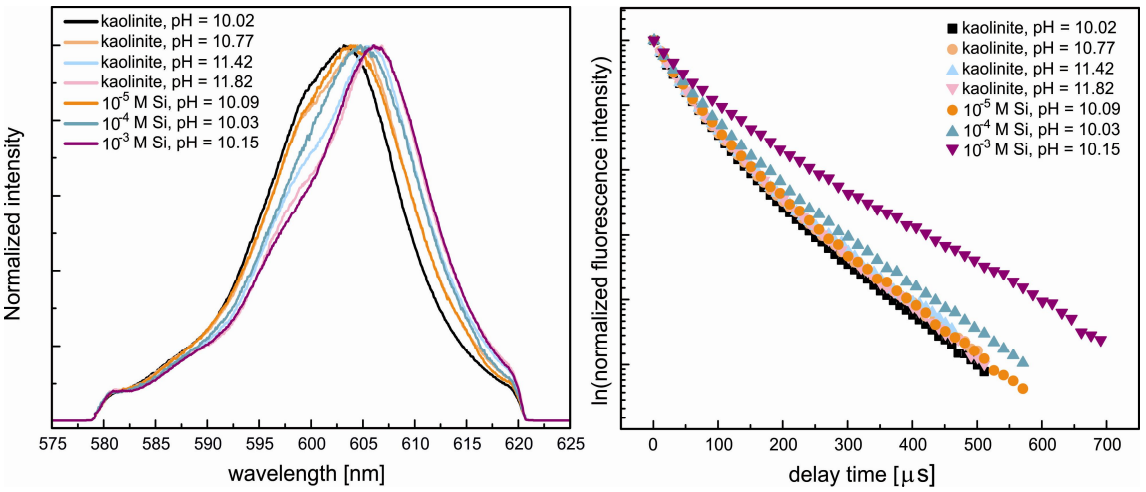

Figure 17: Curium emission spectra (left) and fluorescence lifetimes (right) in kaolinite suspensions with and without silicon addition.

The emission spectra with added silicon at constant pH show a very similar spectral evolution as found in kaolinite suspensions when increasing the pH. However, the fluorescence lifetimes increase from 132 ± 5 µs in pure kaolinite suspensions to 137 µs and 174 µs upon addition of 10^{-4} M and 10^{-3} M Si to the kaolinite suspensions, respectively. In terms of H_2O entities in the first hydration sphere of the curium ion, the increase in lifetimes corresponds to a reduction of the number or H_2O molecules by approximately one from 4.0 in the pure kaolinite suspensions to 2.9 for the highest Si addition. The reason for this increasing lifetime is difficult to explain, especially as no absolute data on the quenching properties of OH^- or the H_3SiO4^- ligand in comparison to H_2O is available. The formation of a curium silicate complex such as the 1:1 $Cm(OSi(OH)_3)^{2+}$ complex found in e.g. Panak et al. [33] and Wang et al. [34] would certainly be accompanied by the displacement of one or several H_2O/OH^- ligands which should increase the fluorescence lifetime. On the other hand O-H groups attached to Si are introduced in the second coordination sphere of the curium ion that may contribute to some quenching of the curium fluorescence [31]. The main difference between the oversaturation experiments and the sorption investigations in the pure kaolinite suspensions besides the silicon concentration is the hydroxyl concentration in solution. In the pure kaolinite suspensions the increase of silicon in solution upon kaolinite dissolution

is accompanied by an increasing concentration of OH^- in the solution as the pH increases. In the oversaturation experiments the silicon concentration was increased but the pH was kept at close to 10, resulting in a constant hydroxyl concentration. This [Si]/[OH^-] concentration difference could be the reason behind the increased fluorescence lifetimes upon silicon addition to the alkaline kaolinite suspensions through the formation of slightly different curium-silicate complexes. For instance complexation between the surface complex $>Cm(OH)(H_2O)_4^+$ and the silicate species $H_4SiO_4/H_3SiO_4^-$ may result in different curium-silicates on the kaolinite surface than complexation between $>Cm(OH)_2(H_2O)_3$ and $H_4SiO_4/H_3SiO_4^-$ would. The degree of curium hydrolysis and the $H_4SiO_4/H_3SiO_4^-$ ratio again are pH dependent. A correct assignment of present species would, however, require a systematic investigation on the influence of silicon vs. OH^- in kaolinite suspensions and should also be accompanied by another spectroscopic technique such as EXAFS for independent validation.

In the present study the underlying mechanism in terms of silicate complexation becomes evident in investigations with α-alumina. Under the assumption that curium is attached to the aluminol sites at the kaolinite surface the oversaturation experiments with silicon were repeated using α-alumina as the sorbent phase. The α-alumina suspensions with 2×10^{-7} M Cm^{3+} were brought to pH > 11 and left to equilibrate for at least three days before the emission spectra and fluorescence lifetimes were recorded. An excess of 10^{-4}-10^{-3} M silicon was added to the samples and TRLFS data was acquired two days later. Similarly to the kaolinite system, a redshift could be observed in the α-alumina suspensions after addition of silicon, together with an increase of luminescence lifetimes from 113 µs without Si to 166 µs with 10^{-3} M Si. The change in fluorescence spectra induced by the addition of silicon to the α-alumina suspension, obtained by subtracting the Cm emission spectrum for pure alpha-alumina without silicon addition from the spectrum where 10^{-3} M Si had been added, greatly resembles the pure component spectrum of the fourth curium complex in alkaline kaolinite suspensions, Figure 18.

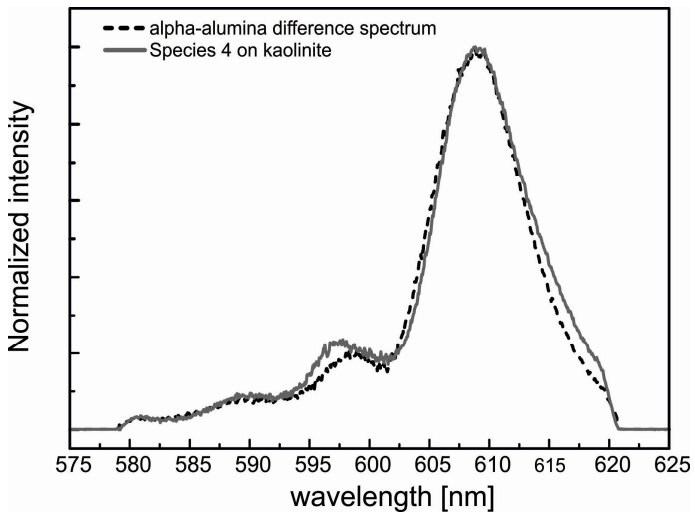

Figure 18: Comparison of the α-alumina difference spectrum and the pure component spectrum of Cm species 4 on the kaolinite surface.

Here, it is clearly evident that silicon influences the ligand-field of curium in both mineral suspensions in a very similar manner. Thus, it is likely that curium is attached to the aluminol groups on both mineral surfaces where it forms a ternary complex with dissolved silicates when the concentration of silicon in solution is high enough.

In conclusion, two modes of attachment (outer and inner sphere) and the complexation with two different inorganic ligands (hydroxyl and silicate) at the mineral surface yielding a total of five complexes (one outer and four inner sphere complexes) are required to fully explain the speciation of curium in the natural kaolinite environment. The study demonstrates the necessity of spectroscopic techniques for a correct assignment of species and interaction mechanisms behind the observed retention of metal ions in batch experiments. Highly alkaline conditions that may arise in nuclear waste disposal sites due to the dissolution of cement that is used in the conditioning of radioactive wastes, increases the solubility of a majority of mineral phases. Dissolution reactions and the relevance of the dissolved species in complexation reactions with long-lived fission products and actinides should, therefore, be examined in detail. How the mobility of the radioelement in question changes upon the change of solution composition is of direct relevance for the safety analysis of radioactive waste repositories.

6.3 NMR results on Eu^{3+} and Y^{3+} adsorption onto γ-alumina and kaolinite (Articles IV, V and unpublished data)

In the NMR investigation care had to be taken when preparing the samples as to not introduce artefacts due to variations in sample pH that influences the degree of protonation of a mineral surface. Thus, all γ-alumina and kaolinite samples were prepared at a constant pH value of 8.0 as explained previously. The influence of suspension pH on the measured NMR spectra was, nevertheless, investigated for the γ-alumina mineral. In Figure 19 proton spectra of γ-alumina samples prepared at different suspension pH values are presented. The spectra are normalized to the same mass [1 mg] of γ-alumina and consequently to the same surface area.

The spectra are characterized by three regions: a shoulder at -0.3 ppm, two resolved peaks at 0.9 and 1.3 ppm and features with chemical shifts at 3.9 ppm and above. The latter proton signals decrease as a function of increasing pH, while the opposite is observed for the -0.3 ppm signal. This is attributed to the deprotonation of surface hydroxyls upon increasing suspension pH. In the acidic pH range the surface of γ-alumina is positively charged due to protonated hydroxyl sites $Al\text{-}OH_2^+$. When the pH is increased these protons dissociate, yielding neutral $Al\text{-}OH^0$ groups that further dissociate to negative $Al\text{-}O^-$ groups in the alkaline pH region. Due to lower shielding of the protonated hydroxyl protons they are observed at higher chemical shifts than the corresponding protons of neutral hydroxyl sites. The 1.3 and 0.9 ppm peaks could be attributed to physisorbed water remaining on the sorbent surface even after drying treatment. These signals also appear in several studies on other mineral surfaces such as fluorapatite, $Ca_5(PO_4)_3F$, [107], gibbsite [108]

and fumed silica (Article IV). The results clearly indicate that suspension pH influences the recorded proton spectra in a significant manner, emphasizing the requirement for a constant pH during adsorption experiments.

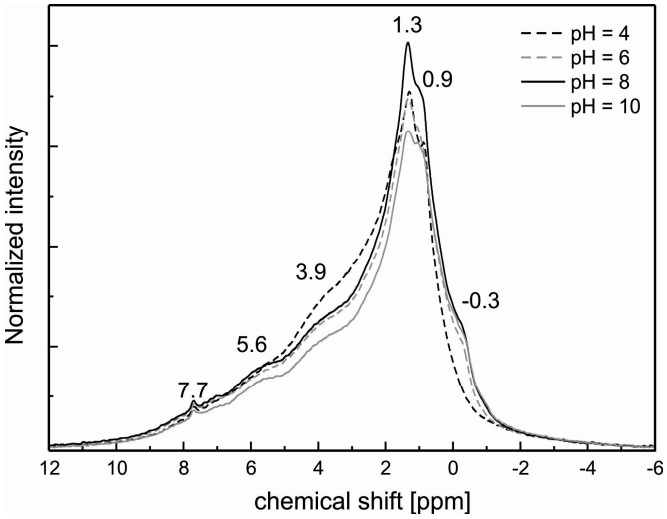

Figure 19: Proton spectra of γ-alumina samples prepared at different suspension pH values.

When yttrium or europium are introduced to the γ-alumina samples, a clear decrease of the proton signal can be discerned due to surface complexation reactions where a proton dissociates from the hydroxyl groups upon metal ion attachment to the surface. This difference, however, is far more pronounced for the paramagnetic europium ion in comparison to diamagnetic yttrium, Figure 20 left. In Figure 20 right, the proton spectra of a pure γ-alumina sample and all samples with added yttrium are shown.

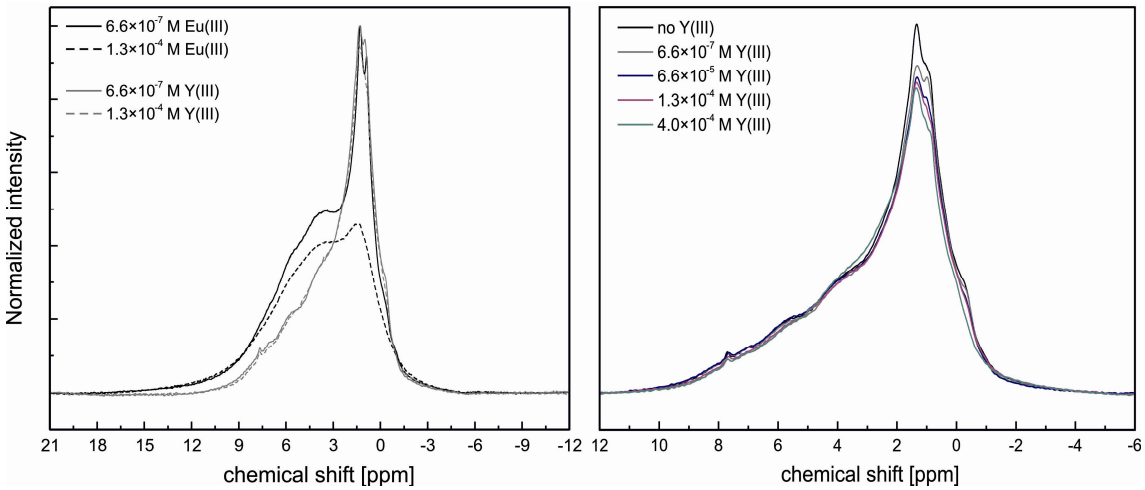

Figure 20: Left – comparison of γ-alumina ^{1}H spectra with europium (black color) and yttrium (gray color). Right - the proton spectra of a pure γ-alumina sample and all samples with added yttrium.

Apart from the visible decrease of the 1.3 and 0.9 ppm bands upon yttrium adsorption no detailed information about the specific bonding of the metal on the mineral surface can be extracted. It is, however, clear that the addition of yttrium removes a notable amount of protons from the γ-alumina surface. The situation is different in the kaolinite samples where the majority of the proton signal stems from the bulk structure $Al_2Si_2O_5(OH)_4$. Just as in the γ-alumina study the Eu^{3+} containing spectra show a greater removal of protons than Y^{3+} from the mineral surface, but the overall effect on the total proton signal is very small. The difference between the spectra with lowest and highest amounts of added metal-ion is 0.72% in case of Y^{3+} and 2.16% in case of Eu^{3+}. This very small difference in proton signal originating from the mineral surface did not allow for normalization of the spectra according to sample mass, but the aluminum data had to be used for normalization purposes as explained in the experimental section. In order to see the spectral changes induced by the sorption reaction at the γ-alumina and kaolinite surfaces, difference spectra were produced. In the γ-alumina study these difference spectra were acquired by subtracting the proton spectra of the samples containing yttrium from that of the unreacted γ-alumina sample. This was not possible in the kaolinite study due to phasing problems which required the unreacted kaolinite sample to be excluded from the data interpretation. Therefore, difference spectra were produced by subtracting the spectra containing higher metal ion concentrations (4×10^{-5} M and 8×10^{-5} M) from the spectrum with the least added amount of metal ion (4×10^{-6} M). Acquired difference spectra are presented in Figure 21 for γ-alumina (left) and kaolinite (right).

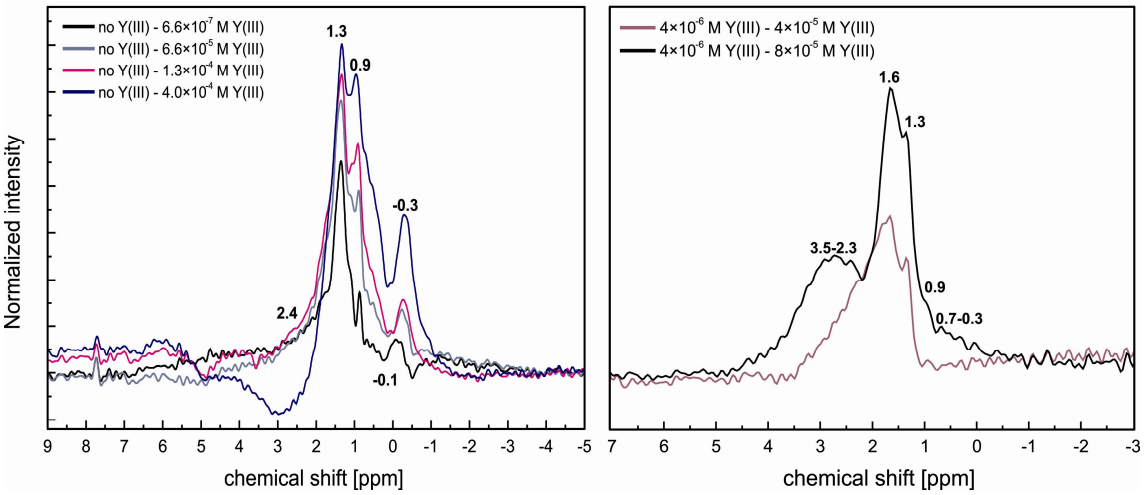

Figure 21: Difference spectra produced by subtraction of proton spectra containing yttrium from either the pure mineral spectrum (γ-alumina study, left) or the spectrum containing the lowest yttrium concentration (kaolinite study, right).

In the γ-alumina difference spectra clear peaks at 1.3, 0.9, -0.1 and -0.3 ppm can be distinguished along with a negative broad feature at approximately 3 ppm. The negative peak is assigned to protons from $Y(OH)_3$, precipitating from oversaturated solutions. The increasing intensity of the signals in the difference spectra corresponding to physisorbed water at 1.3 and 0.9 ppm can be seen to increase as a function of increasing yttrium

concentration. This could be attributed to the decreasing number of available surface sites for hydrogen bond formation between water molecules and surface hydroxyl groups upon yttrium adsorption onto the surface. These signals also appear in the kaolinite difference spectra indicating that some physisorbed water remains on the mineral surface even though the drying treatment was done at higher temperature (180°C) and lower pressure (0.2 mTorr) in comparison to the γ-alumina study (150°C, 20 mTorr).

The proton signals from the γ-alumina sample could be assigned in analogy to a study by DeCanio et al. [109] where peak positions at -0.3, 0.0, 0.9, 1.2, 1.5 and 2.4 ppm had been resolved after deuteration and calcination of a γ-alumina mineral. In their study the peaks at -0.3 ppm and 2.4 ppm were assigned to the most basic and acidic OH-groups on the γ-alumina surface, respectively. Peaks at 1.5, 0.9, and 0.0 ppm where assigned to hydroxyl groups with intermediate acidity while the 1.2 ppm peak was assigned to non-hydrogen bonded water on the γ-alumina surface. The peak at 2.4 ppm is not visible in the difference spectra shown in Figure 21, indicating that the most acidic protons corresponding to bridging hydroxyls linking three aluminum cations in octahedral positions are not exchanged upon yttrium sorption to the surface. These hydroxyl groups are denoted III in the Knözinger and Ratnasamy model presented in Figure 6. The most basic protons belonging to terminal hydroxyls coordinated to a single tetrahedral Al^{3+} cation (Ia) or a single octahedral Al^{3+} cation (Ib) are assigned to signals with chemical shifts around and below zero ppm. These protons are being removed by complexation of the yttrium ion along with hydroxyls of intermediate acidity or basicity with chemical shifts above zero ppm. These are bridging OH-groups linking a tetrahedral and an octahedral aluminum cation (IIa) or two octahedral cations (IIb). When comparing the difference spectrum obtained in the γ-alumina study with the kaolinite one, similarities with regards to chemical shifts in the 1.3-0.0 ppm region can be observed, Figure 22.

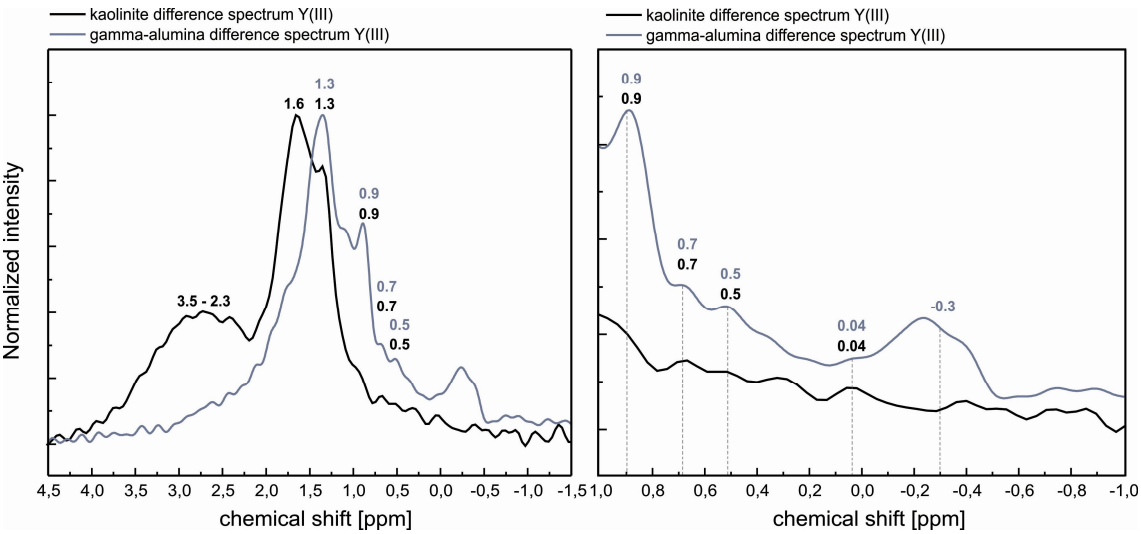

Figure 22: Comparison of difference spectra obtained for γ-alumina and kaolinite (left). The 1-(-1) ppm region of the spectra is illustrated on the right.

Identical peak positions at 1.3, 0.9, 0.7 and 0.5 ppm are resolved in both alumina and kaolinite spectra and the very similar features visible in the magnification of the 1-(-1) ppm region (Figure 22, right) indicate very similar sorption sites between 0.7-0.0 ppm. These peaks appear to be a superposition of multiple proton signals with very similar chemical shifts. Due to the low concentration of these sites and the small shift in reference to TMS, typical for basic protons, these signals are likely to stem from singly coordinated Al_{VI}-OH groups. The presence of multiple signals can be understood when considering these surface groups to have slightly different O-H bond distances. According to DFT calculations comprising the most relevant surface planes on γ-alumina [110], the bond-lengths e.g. of Al_{VI}-OH groups vary slightly depending on what surface they are attached to. A longer bond length produces a slightly lower electron density at the proton, which consequently results in a slightly lower shielding of the proton and the occurrence of this proton signal at higher chemical shifts compared with the signal from a corresponding OH-group with a shorter O-H distance.

The presence of multiple similar sorption sites on the kaolinite surface can be confirmed in TRLFS experiments performed on a Cm^{3+} wet-paste sample (where most of the liquid is removed) at pH 7. In the investigations curium excitation was done directly to the emitting f-state using excitation wavelengths from 599 to 606 nm. Instead of acquiring an emission spectrum corresponding to one curium species, multiple emission spectra with very small energy differences were obtained. These are plotted together with the deconvoluted pure component spectrum of the second inner sphere complex on the kaolinite surface in Figure 23.

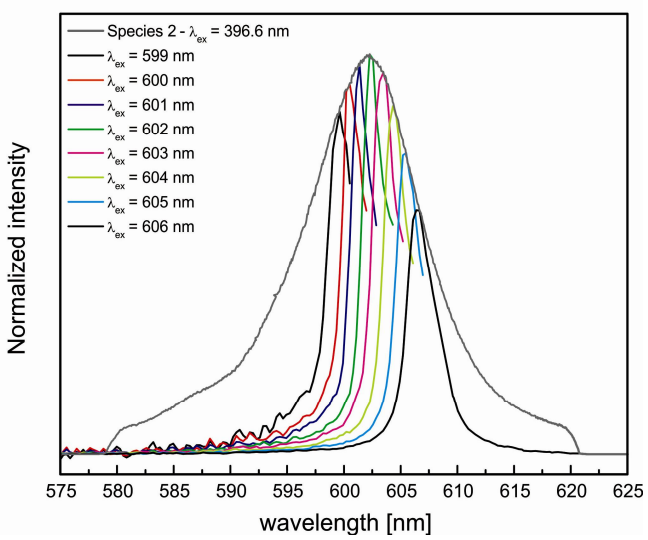

Figure 23: Illustration of the presence of multiple similar curium species at the kaolinite surface obtained in direct excitation experiments of a curium wet paste sample at pH 7. The obtained emission spectra are compared to the pure component spectrum of the second surface complex on the kaolinite surface.

This implies that the extracted pure component spectra are averages of the multiple similar curium species that according to the NMR investigations arise from metal ion attachment to a multitude of chemically very similar surface sites. In other words, the curium species in terms of coordination and hydration water/OH^- entities in the first coordination sphere can be considered identical in all cases but the attachment of the ion onto surface groups with slightly different chemical surroundings influences the curium crystal field states to a slightly different extent so that a multitude of emission spectra are collected.

A similar broad distribution of proton signals is harder to detect in the higher chemical shift regions, where the proton intensity is much greater. The proton intensity between 0.9 and 1.3 ppm, which is very similar in both the kaolinite and γ-alumina study is assigned in accordance with the study by DeCanio et al. [109] to arise from doubly coordinated hydroxyls $(Al_{VI})_2$–OH. The peak at 1.6 ppm and the broad feature in the chemical shift region 2.3-3.5 ppm is only present in the kaolinite spectra. Data on kaolinite proton signals have been reported over a rather broad range of chemical shifts. Wang et al. [111] assigned signals at 2.4-3.0 ppm to the inner surface hydroxyls i.e. doubly coordinated hydroxyls on the exposed aluminum hydroxide basal surface of kaolinite. Fitzgerald et al. [112] made a similar assignment of their pyrophyllite mineral where the 2.4 ppm peak was assigned to OH groups in the gibbsite-like AlOH layer. Furthermore, structural proton signals from the mineral gibbsite have been observed over a rather large range of chemical shifts between 1.8-5.8 ppm [108, 113]. Therefore, the observed signals in the kaolinite difference spectrum (1.6-3.5 ppm) could be ascribed to doubly coordinated hydroxyls with varying acid strengths on the gibbsite-like basal plane of kaolinite. Proton signals from the Al-OH-Si groups have been reported at higher chemical shifts [112, 114] while Si-OH groups are mostly deprotonated at pH 8.0 [115, 116] and will not show up in the recorded proton spectra.

In summary, metal ion sorption onto γ-alumina occurs at both singly and doubly coordinated hydroxyl sites. Singly coordinated Al-OH groups on the kaolinite edge surfaces participate in the metal ion complexation reaction. In addition the results indicate that the gibbsite-like basal plane is available for trivalent metal-ion attachment. Involvement of the kaolinite surface groups Si-OH and Al-OH-Si must be extracted in other type of investigations or alternatively at much lower suspension pH values, where these surface groups are protonated and, thus, visible in ^1H NMR spectra. Data obtained in the NMR investigations show in combination with TRLFS results that multiple species exist on the kaolinite surface due to attachment of the metal at surface hydroxyls with slightly different chemical surroundings. Finally, the comparison of difference spectra show the presence of very similar sorption sites on the different mineral phases kaolinite and γ-alumina, thus, confirming that aluminum oxides can to some extent be used as model phases for the more complex aluminosilicate minerals.

7 Conclusions

The aim of this study has been to elucidate the retention behavior of trivalent actinides on mineral surfaces at the molecular level. Detailed understanding of the reaction mechanisms at the solid/water interface must be the foundation for any reliable long-term safety prognosis of nuclear waste repositories. The study has demonstrated the importance of spectroscopic investigations for understanding the chemistry behind the acquired sorption distribution coefficients that are being used in thermodynamic modeling of radionuclide migration in the geosphere. New spectroscopic data has been obtained in NMR investigations on the various surface hydroxyl groups on γ-alumina and kaolinite and information on the affinity of these surface hydroxyls towards the trivalent metal has been acquired. In addition, TRLFS investigations on the speciation of trivalent actinides in gibbsite and kaolinite suspensions were applied. Various attachment modes of curium at the mineral surfaces and the presence of multiple curium species were identified in both mineral suspensions over a broad pH range.

The most important take-away message of this thesis is that the dynamics of mineral surfaces in terms of dissolution and precipitation must not be neglected in any type of investigations where experimental conditions vary throughout the experiment. Not only can the dissolved mineral components function as complexing ligands in the aqueous environment, but the possibility of metal ion incorporation by processes that are not driven by thermodynamic stability of the mixed phase, i.e. in processes where solid/solution formation is favored, must be taken into account. Actinide incorporation into minerals with dynamic surfaces is quite well known: Calcium carbonates such as vaterite and calcite have for instance been shown to form thermodynamically driven solid/solutions with trivalent actinides and lanthanides [117-119]. In these studies the trivalent metal has substituted the host cation in the crystal lattice and the incorporation has been shown to be favored over surface complexation as a function of contact time. In the present study incorporation was shown to occur when the trivalent metal attached to the aluminum hydroxide surface became covered by a precipitating aluminum phase from oversaturated solutions. Here, no substitution of aluminum by the actinide in the mineral lattice occurs and the curium incorporation is released when solution conditions are altered, such that aluminum solubility increases resulting in dissolution of the precipitate.

Batch sorption investigations provide very limited information on the retention mechanisms in the investigated systems. They are, however, necessary to perform as they provide the baseline on the metal ion uptake that would be difficult to obtain e.g. from the TRLFS spectra. Retention might be significant under conditions where TRLFS data show only the presence of aqueous species, thus, the limitations of all methods taken separately and the power gained by combining them must be acknowledged.

Finally, NMR has proven to be a powerful tool in the determination of surface hydroxyl sites, in a series of initial experiments. The method allows for identification of surface hydroxyl groups involved in the sorption processes, information that is not easily accessible by other techniques. An unambiguous assignment of these hydroxyl groups would be greatly facilitated when NMR spectra were simulated for the predicted surface hydroxyls. Simulated ^{27}Al NMR spectra are already available for some aluminum oxide phases [120] and it is to be expected that simulated ^{1}H data on the various surface hydroxyl protons will not be very far behind and available in the near future.

8 References

1 National Research Council (1957) *The disposal of radioactive waste on land*. The National Academies Press, Washington, DC.

2 Posiva Oy (1996) Final disposal of spent nuclear fuel in the Finnish bedrock - Technical research and development in the period 1993 - 1996. Helsinki, POSIVA-96-14 (in Finnish).

3 Swedish Nuclear Fuel Supply Co/Division KBS (SKBF/KBS) (1983) KBS 3 - Final storage of spent nuclear fuel - KBS-3, Summary, SKB report number Art716 5.

4 Swedish Nuclear Fuel Supply Co/Division KBS (SKBF/KBS) (1983) KBS 3 - Final storage of spent nuclear fuel - KBS-3, III Barriers, SKB report number Art716 3.

5 IAEA (2004) Implications of partitioning and transmutation in radioactive waste management, IAEA Technical report series no. 435.

6 Streffer C., Gethmann C. F., Kamp G., Kröger W., Rehbinder E., Renn O. and Röhlig K.-J. (2011) *Radioactive waste - Technical and normative aspects of its disposal, Ethics of science and technology assessment*, Vol. 38, Springer-Verlag Berlin Heidelberg.

7 Colonna N., Belloni F., Berthoumieux E., Calviani M., Domingo-Pardo C., Guerrero C., Karadimos D., Lederer C., Massimi C., Paradela C., Plag R., Praenam J. and Sarmenton R. (2010) Advanced nuclear energy systems and the need of accurate nuclear data: the n_TOF project at CERN. *Energy Environ. Sci.* **3**, 1910–1917.

8 Henri M., Jolivet J. P. and Livage J. (1992) Aqueous chemistry of metal cations: Hydrolysis, condensation and complexation. *Structure and Bonding*, **77**, 155-206.

9 Morss L. R., Edelstein N. M. and Fuger J. (Eds.) (2006) *The chemistry of the actinides and transactinide elements*, 3rd edition, Volume 4, Springer, Netherlands.

10 Kimura T. and Choppin G. R. (1994) Luminescence study on determination of the hydration number of Cm(III). *J. Alloys Compd.* **213-214**, 313-317.

11 Lindqvist-Reis P., Klenze R., Schubert G. and Fanghänel T. (2005) Hydration of Cm^{3+} in aqueous solution from 20 to 200 °C. A time-resolved laser fluorescence spectroscopy study. *J. Phys. Chem. B* **109**, 3077-3083.

12 Skanthakumar S., Antonio M. R., Wilson R. E. and Soderholm L. (2007) The Curium aqua ion. *Inorg. Chem.* **46**, 3485-3491.

13 Lindqvist-Reis P., Apostolidis C., Rebizant J., Morgenstern A., Klenze R., Walter O., Fanghänel T. and Haire R. G. (2007) The structures and optical spectra of hydrated transplutonium ions in the solid state and in solution. *Angew. Chem., Int. Ed.* **46**, 919-922.

14 Yang T. and Bursten B. E. (2006) Speciation of the curium(III) ion in aqueous solution: A combined study by quantum chemistry and molecular dynamics simulation. *Inorg. Chem.* **45**, 5291-5301.

15 Gschneidner K. A., Eyring LeRoy. Jr., Lander G. H. and Choppin G. R. (Eds.) (1994) Lanthanides/Actinides: Chemistry. *Handbook on the physics and chemistry of rare earths,* volume 18, Elsevier Science B. V.

16 Baes C. F. Jr. and Mesmer R. E. (1976) *The hydrolysis of cations*. John Wiley & Sons, Inc. New York.

17 Choppin G., Liljenzin J.-O. and Rydberg J. (2002) *Radiochemistry and nuclear chemistry*, 3rd edition, Butterworth-Heinemann, Woburn, MA.

18 Fanghänel Th. and Neck V. (2002) Aquatic chemistry and solubility phenomena of actinide oxides/hydroxides. *Pure Appl. Chem*. **74**, 1895–1907.

19 Runde W. (2000) The chemical interactions of actinides in the environment, *Los Alamos Science*, **26**, 392-411.

20 Parkhurst D. L. and Appelo C. A. J. (1999) User's guide to PHREEQC (Version2) - A computer program for speciation, batch-reaction, one-dimensional transport, and inverse geochemical calculations. *Water-Resources Investigations Report 99-4259*, US Geological Survey, Denver, Colorado.

21 Duro L., Grivé M., Gaona X., Domènech C., Colás E., Montoya V. and Bruno J. (2007) Development of the ThermoChimie thermodynamic data base. ANDRA Report C.RP.0ENQ.07.0001.

22 Grenthe I., Fuger J., Konings R. J. M., Lemire R. J., Muller A. B., Nguyen-Trung C. and Wanner H. (OECD/NEA) (1992) *Chemical thermodynamics Vol. 1. Chemical thermodynamics of uranium*. Elsevier Science Publ., North-Holland, Amsterdam.

23 Silva R. J., Bidoglio G., Rand M. H., Robouch P., Wanner H. and Puigdomenech I. (OECD/NEA) (1995) *Chemical thermodynamics Vol. 2. Chemical thermodynamics of americium*. Elsevier Science Publ., North-Holland, Amsterdam.

24 Lemire R. J., Fuger J., Nitsche H., Potter P., Rand M. H., Rydberg J., Spahiu K., Sullivan J. C., Ullman W. J., Vitorge P. and Wanner H. (OECD/NEA) (2001) *Chemical thermodynamics Vol. 4. Chemical thermodynamics of neptunium and plutonium*. Elsevier Science Publ., North-Holland, Amsterdam.

25 Moulin V. and Ouzounian G. (1992) Role of colloids and humic substances in the transport of radio-elements through the geosphere. *Appl. Geochem*. **7**, 179-186.

26 Pitkänen P., Snellman M. and Leino-Forsman H. (1994) Aspects affecting the chemistry of bedrock groundwaters: Results from Finnish site investigations for nuclear waste disposal. *Future groundwater resources at risk*, IAHS Publ. **222**, 355-362.

27 Gehör S., Karhu J., Kärki A., Löfman J., Pitkänen P., Ruotsalainen P. and Taikina-aho O. (2002) Fracture calcites at Olkiluoto, evidence from quaternary infills for palaeohydrogeology. Posiva Oy, Olkiluoto, Finland. Working report **2002-03**.

28 Kärki A. and Lahdenperä, T. (2002) Eurajoki, Olkiluoto, low temperature fracture minerals in drill core samples OL-KR2, -KR3, -KR4, -KR5, -KR7, -KR8 and -KR10. Posiva Oy, Olkiluoto, Finland. Working Report **2002-04** (in Finnish).

29 Pitkänen P., Partamies S. and Luukkonen A. (2003) Hydrogeochemical interpretation of baseline groundwater conditions at the Olkiluoto site. Posiva Oy, Olkiluoto, Finland. Working Report **2003-07.**

30 Choppin G. R. (1971) Structure and thermodynamics of lanthanide and actinide complexes in solution. *Pure Appl. Chem*. **27**, 23-41.

31 Jensen M. P. and Choppin G. R. (1996) Complexation of europium(III) by aqueous orthosilicic acid. *Radiochim. Acta* **72**, 143-150.

32 Wadsak W., Hrnecek E. and Irlweck K. (2000) Formation of americium(III) complexes with aqueous silicic acid. *Radiochim. Acta* **88**, 61-64.

33 Panak P. J., Kim M. A., Klenze R., Kim J. I. and Fanghänel Th. (2005) Complexation of Cm(III) with aqueous silicic acid. *Radiochim. Acta* **93**, 133-139.

34 Wang Z., Felmy A. R., Xia Y. X., Qafoku O., Yantassee W. and Cho H. (2005) Complexation of Cm(III)/Eu(III) with silicates in basic solutions. *Radiochim. Acta* **93**, 741-748.

35 Thakur P., Singh D. K. and Choppin G. R. (2007) Polymerization study of o-$Si(OH)_4$ and complexation with Am(III), Eu(III) and Cm(III). *Inorg. Chim. Acta* **360**, 3705–3711.

36 U.S. Department of Energy (2007) Basic Research Needs for Geosciences: Facilitating 21st Century Energy Systems, BES Workshop on Basic Research Needs for Geosciences.

37 Geckeis H. and Rabung Th. (2008) Actinide geochemistry: From the molecular level to the real system. *J. Contam. Hydrol.* **102**, 187–195.

38 Sparks D. L. (2003) *Environmental soil chemistry*, 2nd edition, Elsevier Science, San Diego, USA.

39 Sposito G. (2008) *The chemistry of soils*, 2nd edition, Oxford University Press, Inc., New York, USA.

40 Stumm W. (1992) *Chemistry of the solid-water interface: Processes at the mineral-water and particle-water interface in natural systems.* John Wiley & Sons, Inc., New York.

41 Bruno J., Bosbach D., Kulik D. and Navrotsky, A. (2007) Chemical thermodynamics of solid solutions of interest in nuclear waste management, Chemical thermodynamics series, volume 10, OECD, Nuclear Energy Agency.

42 Parks G. A. (1990) Surface energy and adsorption at mineral-water interfaces: an introduction, *Reviews in Mineralogy, Vol 23: Mineral water interface geochemistry*. The mineralogical society of America, Washington D.C., USA.

43 Waite T. D., Davis J. A., Payne T. E., Waychunas G. A. and Xu N. (1994) Uranium(VI) adsorption to ferrihydrite: Application of a surface complexation model. *Geochim. Cosmochim. Acta* **58**, 5465–5478.

44 Naveau A., Monteil-Rivera F., Dumonceau J. and Boudesocque S. (2005) Sorption of europium on a goethite surface: influence of background electrolyte. *J. Contam. Hydrol.* **77**, 1-16.

45 Marques Fernandes M., Stumpf T., Baeyens B., Walther C. and Bradbury M. H. (2010) Spectroscopic identification of ternary Cm-carbonate surface complexes. *Environ. Sci. Technol.* **44**, 921–927.

46 O'Day P. A. (1999) Molecular environmental geochemistry. *Rev. Geophys.* **37**, 249-274.

47 Kosmulski M. (2001) *Chemical Properties of Material Surfaces*, Marcel Dekker Inc.

48 Koretsky C. (2000) The significance of surface complexation reactions in hydrologic systems: a geochemist's perspective. *J. Hydrol.* **230**, 127–171.

49 Hiemstra T., Han Yong and Van Riemsdijk W. H. (1999) Interfacial charging phenomena of aluminum (hydr)oxides. *Langmuir* **15**, 5942-5955.

50 Ma C., Chang Y., Ye W., Shang W. and Wang C. (2008) Supercritical preparation of hexagonal γ-alumina nanosheets and its electrocatalytic properties. *J. Colloid Interface Sci*. **317**, 148–154.

51 Knözinger H. and Ratnasamy P. (1978) Catalytic aluminas: Surface models and characterization of surface sites. *Catal. Rev*. **17**, 31–70.

52 Bergaya F., Theng B. K. G. and Lagaly G. (Eds.) (2006) *Handbook of clay science*, 1st edition, Elsevier Science, The Netherlands.

53 Zachara J. M. and McKinley J. P. (1993) Influence of hydrolysis on the sorption of metal cations by smectites: Important edge coordination reactions. *Aquat. Sci*. **55**, 250-261.

54 McKinley J. P., Zachara J. M., Smith S. C. and Turner G. D. (1995) The influence of uranyl hydrolysis and multiple site-binding reactions on adsorption of U(VI) to montmorillonite. *Clays Clay Miner*. **43**, 586-598.

55 Stumm W. and Morgan J. J. (1995) *Aquatic chemistry – Chemical equilibria and rates in natural waters*, 3rd edition, John Wiley & Sons Inc., New York, USA.

56 Staunton S. (1994) Adsorption of radiocesium on various soils – interpretation and consequences of the effects of soil-solution ratio and solution composition on the distribution coefficient. *Eur. J. Soil Sci.* **45**, 409-418.

57 United States Environmental Protection Agency (1999) Understanding variations in partition coefficient K_d, values - Volume I: The K_d model, methods of measurement, and application of chemical reaction codes. EPA report 402-R-99-004A.

58 Lee S., Fenter P., Park C., Sturchio N. C. and Nagy K. L. (2010) Hydrated cation speciation at the muscovite (001)-water interface. *Langmuir* **26**, 16647–16651.

59 Degueldre C., Ulrich H. J. and Silby H. (1994) Sorption of ^{241}Am onto montmorillonite, illite and hematite colloids. *Radiochim. Acta* **65**, 173-179.

60 Stumpf S., Stumpf Th., Lützenkirchen J., Walther C. and Fanghänel Th. (2008) Immobilization of trivalent actinides by sorption onto quartz and incorporation into siliceous bulk: Investigations by TRLFS. *J. Colloid Interface Sci*. **318**, 5-14.

61 Dzombak D. A. and Morel M. M. (1990) *Surface complexation modeling: hydrous ferric oxide*. John Wiley & Sons, New York, USA.

62 Mathur S. S. and Dzombak D. A. (2006) Chapter 16: Surface complexation modeling: goethite, *Interface Science and Technology*, Vol 11; J. Lützenkirchen, Ed. Elsevier Ltd. Amsterdam, 443–468.

63 Bradbury M. H. and Baeyens B. (2005) Modelling the sorption of Mn(II), Co(II), Ni(II), Zn(II), Cd(II), Eu(III), Am(III), Sn(IV), Th(IV), Np(V) and U(VI) on montmorillonite: linear free energy relationships and estimates of surface binding constants for some selected heavy metals and actinides. *Geochim. Cosmochim. Acta* **69**, 875–892.

64 Bradbury M. H. and Baeyens B. (2009) Sorption modelling on illite. Part II: Actinide sorption and linear free energy relationships. *Geochim. Cosmochim. Acta* **73**, 1004–1013.

65 Gu X. and Evans L. J. (2008) Surface complexation modelling of Cd(II), Cu(II), Ni(II), Pb(II) and Zn(II) adsorption onto kaolinite. *Geochim. Cosmochim. Acta* **72**, 267–276.

66 Bünzli J.-C. G. and Choppin G. R. (1989) *Lanthanide Probes in Life, Chemical and Earth Sciences, Theory and Practice*, Elsevier Science Publisher, Amsterdam.

67 Lakowicz J. R. (2006) *Principles of fluorescence spectroscopy*, 3rd edition, Springer Science + Business Media LLC, New York, USA.

68 Wimmer H. (1992) Laser-induzierte optische Spektroskopie zur Speziation von f- Elementen in natürlichen aquatischen Systemen, Ph.D. thesis, Institut für Radiochemie, Technische Universität München, Germany.

69 Hüfner S. (1978) *Optical spectra of transparent rare earth compounds*, Academic Press, New York.

70 Carnall W. T. and Rajnak K. (1975) Electronic energy level and intensity correlations in the spectra of the trivalent actinide aquo ions. II. Cm^{3+}. *J. Chem. Phys.* **63**, 3510-3514.

71 Beitz J. V. (1991) Laser-induced fluorescence studies of Cm^{3+} complexes in solution. *Radiochim. Acta* **52/53**, 35-39.

72 Kropp J. L and Windsor M. W. (1965) Luminescence and energy transfer in solutions of rare-earth complexes. I. Enhancement of fluorescence by deuterium substitution. *J. Chem. Phys.* **42**, 1599-1608.

73 Stein G. and Würzberg E. (1975) Energy gap law in the solvent isotope effect on radiationless transitions of rare earth ions. *J. Chem. Phys.* **62**, 208-213.

74 Stumpf Th., Bauer A., Coppin F., Fanghänel Th. and Kim J. I. (2002) Inner-sphere, outer-sphere and ternary surface complexes: a TRLFS study of the sorption process of Eu(III) onto smectite and kaolinite. *Radiochim. Acta* **90**, 345-349.

75 Hartmann E., Baeyens B., Bradbury M. H., Geckeis H. and Stumpf Th. (2008) A spectroscopic characterization and quantification of M(III)/Clay mineral outer-sphere complexes. *Environ. Sci. Technol.* **42**, 7601–7606.

76 Akitt J. W. (1973) *N.M.R. and Chemistry – An introduction to nuclear magnetic resonance spectroscopy*, Chapman and Hall Ltd, London.

77 Williams D. A. R. (1986) *Nuclear magnetic resonance spectroscopy*, John Wiley & Sons, London.

78 Gemmecker G. (1999) Basis Principles of FT NMR in Advanced NMR spectroscopy, University of Wisconsin, Madison.

79 Drago R. S., Zink J. I., Richman R. M. and Perry W. D. (1974) Theory of isotropic shifts in the NMR of paramagnetic materials. *J. Chem. Educ*. **51**, 371-376.

80 Woessner D. E. (1980) An NMR investigation into the range of the surface effect on the rotation of water molecules. *J. Magn. Reson.* **39**, 297–308.

81 Grüne M. and Müller-Warmuth W. (1995) The importance of paramagnetic impurities to the nuclear magnetic resonance relaxation of ion-conducting glasses. *Solid State Nucl. Magn. Reson.* **5**, 145-150.

82 Dai K. H. and Johnson C. E. (1999) Applicability of solid-state ^{13}C CP/MAS NMR analysis in Spodosols: chemical removal of magnetic materials. *Geoderma* **93**, 289-310.

83 Bray C. L., Bryant R. G., Cox M. J., Ferrante G., Goddard Y. A., Sur S. K. and Hornak J. P. J. (2009) The H-1 nuclear magnetic resonance spin-lattice relaxation rate of some hydrated synthetic and natural sands. *Environ. Eng. Geophys.* **14**, 49-61.

84 King A. R., Wolfe J. P. and Ballard R. L. (1972) NMR of nuclei near a paramagnetic impurity in crystals. *Phys. Rev. Lett.* **28**, 1099–1102.

85 Grey C. P., Dobson C. M., Cheetham A. K. and Jakeman R. J. B. (1989) Studies of rare-earth stannates by ^{119}Sn MAS NMR. The use of paramagnetic shift probes in the solid state. *J. Am. Chem. Soc.* **111**, 505-511.

86 Harazono T., Adachi R., Kijima N. and Watanabe T. (1999) ^{89}Y MAS NMR in red phosphor, Eu-doped Y_2O_2S. Assignment of peaks shifted by paramagnetic Eu^{3+}, spin lattice relaxation time, and Eu distribution. *Bull. Chem. Soc. Jpn.* **72**, 2655-2664.

87 Ganapathy S., Naito A. and McDowell C. A. (1981) Paramagnetic doping as an aid in obtaining high-resolution carbon-13 NMR spectra of biomolecules in the solid state. *J. Am. Chem. Soc.* **103**, 6011–6015.

88 Fyfe C.A. (1983) *Solid state NMR for chemists*, C.F.C. press, Ontario, Canada.

89 Duer M. J. (2004) *Introduction to solid-state NMR spectroscopy*, Blackwell Publishing Ltd, Oxford, UK.

90 Farrar T. C. and Becker E. D. (1971) *Pulse and Fourier transform NMR – Introduction to theory and methods*, Academic Press, Inc. New York, USA.

91 Zorin V. E., Brown S. P. and Hodgkinson P. (2006) Origins of linewidth in ^{1}H magic-angle spinning NMR. *J. Chem. Phys.* **125**, 144508.

92 MacKenzie K. J. D. and Smith M. E. (2002) *Multinuclear solid-state NMR of inorganic materials*, 1st edition, Elsevier Science Ltd, Oxford, UK.

93 Engelhardt G. and Michel D. (1987) *High-resolution solid-state NMR of silicates and zeolites*, John Wiley & Sons Ltd, Chichester, UK.

94 Chan J. C. C. (Ed) (2012) *Solid state NMR, Topics in current chemistry*, Vol. 306, Springer Verlag Berlin Heidelberg.

95 Bauer A. and Berger G. (1998) Kaolinite and smectite dissolution rate in high molar KOH solutions at 35 and 80°C. *Appl. Geochem.* **13**, 905–916.

96 Coppin F., Berger G., Bauer A., Castet S. and Loubet M. (2002) Sorption of lanthanides on smectite and kaolinite. Chem. Geol. 182, 57–68.

97 Rabung Th., Pierret M. C., Bauer A., Geckeis H., Bradbury M. H. and Baeyens B. (2005) Sorption of Eu(III)/Cm(III) on Ca-montmorillonite and Na-illite. Part 1: Batch sorption and time-resolved laser fluorescence spectroscopy experiments. *Geochim. Cosmochim. Acta* **69**, 5393–5402.

98 El-Bayaa A. A., Badawy N. A. and Abd AlKhalik E. (2009) Effect of ionic strength on the adsorption of copper and chromium ions by vermiculite pure clay mineral. *J. Hazard. Mater.* **170**, 1204–1209.

99 Schindler P. W. and Stumm W. (1987) *Aquatic surface chemistry*, Wiley-Interscience, New York, USA.

100 Geckeis H. and Rabung Th. (2002) Solid-water interface reactions of polyvalent metal ions at iron oxide surfaces, *Encyclopedia of Surface and Colloid Science*, A. Hubbard (Ed.), Marcel Dekker, New York, USA.

101 Brown D. E., Campbell T. W. and Moore R. N. (1989) Automated phase correction of FT NMR spectra by baseline optimization. *J. Magn. Reson.* **85**, 15-23.

102 Brantley S. L., Kubicki J. D. and White A. F. (Eds.) (2008) *Kinetics of Water-Rock Interaction*, Springer, New York.

103 Mattigod S. V., Gibali A. S. and Page A. L. (1979) Effect of ionic strength and ion pair formation on the adsorption of nickel by kaolinite. *Clays Clay Miner*. **27**, 411-416.

104 Turan P., Doğan M. and Alkan M. (2007) Uptake of trivalent chromium ions from aqueous solutions using kaolinite. *J. Hazard. Mater*. **148**, 56-63.

105 Seward T. M., Henderson C. M. B. and Charnock J. M. (2000) Indium(III) chloride complexing and solvation in hydrothermal solutions to 350°C: an EXAFS study. *Chem. Geol*. **167**, 117-127.

106 Wang Z., Felmy A. R., Xia Y. X. and Mason M. J. (2003) A fluorescence spectroscopic study on the speciation of Cm(III) and Eu(III) in the presence of organic chelates in highly basic solutions. *Radiochim. Acta* **91**, 329-337.

107 Sandström D. E., Jarlbring M., Antzutkin O. N. and Forsling W. (2006) A spectroscopic study of calcium surface sites and adsorbed iron species at aqueous fluorapatite by means of ^{1}H and ^{31}P MAS NMR. *Langmuir* **22**, 11060–11064.

108 Xue X. and Kanzaki M. (2007) High-pressure δ-$Al(OH)_3$ and δ-AlOOH phases and isostructural hydroxides/oxyhydroxides: New structural insights from high-resolution ^{1}H and ^{27}Al NMR. *J. Phys. Chem. B* **111**, 13156-13166.

109 DeCanio E. C., Edwards J. C. and Bruno J. W. (1994) Solid state ^{1}H MAS NMR characterization of γ-alumina and modified γ-aluminas. *J. Catal*. **148**, 76-83.

110 Digne M., Sautet P., Raybaud P., Euzen P. and Toulhoat H. (2004) Use of DFT to achieve a rational understanding of acid-basic properties of γ-alumina surfaces. *J. Catal*. **226**, 54-68.

111 Wang L., Wu D., Yuan P., Chen Z. and Chen Z. (2002) ^{1}H MAS NMR spectra of kaolinite/formamide intercalation compound. *Chin. Sci. Bull.* **47**, 504-508.

112 Fitzgerald J. J., Hamza A. I., Dec S. F. and Bronnimann C. E. (1996) Solid-state ^{27}Al and ^{29}Si NMR and ^{1}H CRAMPS studies of the thermal transformation of the 2:1 phyllosilicate pyrophyllite. *J. Phys. Chem.* **100**, 17351-17360.

113 Piedra G., Fitzgerald J. J., Dando N., Dec S. F. and Maciel G. E. (1996) Solid-state ^{1}H NMR studies of aluminum oxide hydroxides and hydroxides. *Inorg. Chem.* **35**, 3474-3478.

114 Hunger M., Freude D. and Pfeifer H. (1991) Magic-angle nuclear magnetic resonance studies of water molecules adsorbed on Brønstedt- and Lewis-acid sites in zeolites and amorphous silica-aluminas. *J. Chem. Soc. Faraday Trans.* **87**, 657-662.

115 Huertas F. J., Chou L. and Wollast R. (1998) Mechanism of kaolinite dissolution at room temperature and pressure: Part 1. Surface speciation. *Geochim. Cosmochim. Acta* **62**, 417-431.

116 Benyahya L. and Garnier J.-M. (1999) Effect of salicylic acid upon trace-metal sorption (CdII, ZnII, CoII, and MnII) onto alumina, silica, and kaolinite as a function of pH. *Environ. Sci. Technol.* **33**, 1398-1407.

117 Stumpf T. and Fanghänel T. (2002) A time-resolved laser fluorescence spectroscopy (TRLFS) study of the interaction of trivalent actinides (Cm(III)) with calcite. *J. Colloid Interface Sci.* **249,** 119-122.

118 Marques Fernandes M., Schmidt M., Stumpf T., Walther C., Bosbach D., Klenze R. and Fanghänel T. (2008) Site-selective time-resolved laser fluorescence spectroscopy of Eu^{3+} in calcite. *J. Colloid Interface Sci.* **321,** 323–331.

119 Schmidt M., Stumpf T., Walther C., Geckeis H. and Fanghänel T. (2010) Phase transformation in $CaCO_3$ polymorphs: A spectroscopic, microscopic and diffraction study. *J. Colloid Interface Sci.* **351**, 50–56.

120 Ferreira A. R., Küçükbenli E., Leitão A. A. and de Gironcoli S. (2011) Ab initio ^{27}Al NMR chemical shifts and quadrupolar parameters for Al_2O_3 phases and their precursors. *Phys. Rev. B* **84**, 235119.